

Performance Analysis of Distributed Intelligent Reflecting Surfaces for Wireless Communications

Diluka Loku Galappaththige, *Student Member, IEEE*, Dhanushka Kudathanthirige, *Student Member, IEEE*, and Gayan Amarasuriya Aruma Baduge, *Senior Member, IEEE*

Abstract

In this paper, a comprehensive performance analysis of a distributed intelligent reflecting surfaces (IRSs)-aided communication system is presented. First, the optimal signal-to-noise ratio (SNR), which is attainable through the direct and reflected channels, is quantified by controlling the phase-shifts of the distributed IRSs. Next, this optimal SNR is statistically characterized by deriving tight approximations to the probability density function (PDF) and cumulative distribution function (CDF) for Nakagami- m fading. Our PDF/CDF analysis is used to derive tight approximations/bounds for the outage probability, achievable rate, and average symbol error rate (SER) in closed-form. To obtain useful insights, the asymptotic outage probability and average SER are derived for the high SNR regime. Thereby, the achievable diversity order and array gains are quantified. Our asymptotic performance analysis reveals that the diversity order can be boosted by using distributed passive IRSs without generating additional electromagnetic (EM) waves via active radio frequency chains. Our asymptotic rate analysis shows that the lower and upper rate bounds converge to an asymptotic limit in large reflecting element regime. Moreover, the transmission impairments are studied by investigating the detrimental effects of phase-shift quantization errors and the spatially correlated fading at the IRSs. Our analysis is validated via Monte-Carlo simulations. We present a rigorous set of numerical results to investigate the performance gains of the proposed system model. Our analytical and numerical results reveal that the performance of single-input single-output wireless systems can be boosted by recycling the EM waves generated by a transmitter through distributed passive IRS reflections to enable constructive signal combining at a receiver.

The authors are with the School of Electrical, Computer, and Biomedical Engineering, Southern Illinois University, Carbondale, IL, USA, Email: {diluka.lg, dhanushka.kudathanthirige, gayan.baduge}@siu.edu. This work in part has been presented at IEEE Global Communication Conference (Globecom), Dec., 2020 [1].

I. INTRODUCTION

Recently, a novel concept of coating physical objects such as building walls and windows within a wireless propagation medium with intelligent reflecting surfaces (IRSs), which can interact with electromagnetic (EM) waves, has emerged [1]–[3]. By invoking the recent research developments of meta-surfaces [4], the feasibility of synthesizing the IRS has been explored [2]. An IRS consists of a large number of passive reflecting elements, which can introduce controllable phase-shifts to incident EM waves. These phase-shifts can be intelligently controlled to enable a constructive addition of EM waves at a desired destination and thereby boosting the signal-to-noise ratio (SNR) of the end-to-end communication. Moreover, the IRS enables recycling of EM waves without generating additional signals via radio-frequency (RF) chains/amplifiers and thus enhancing the energy efficiency. The current state-of-the-art wireless systems, including conventional communication systems such as massive multiple-input multiple-output (MIMO), millimeter wave (mmWave) communication, and ultra-dense deployments of small cells consume a high amount of energy and a considerable hardware implementation cost [5]. The emerging mmWave communications may suffer from high path-losses, penetration losses, and signal blockages. To this end, IRS-aided communication systems can potentially address the need of greener, more cost effective, and more sustainable wireless connectivity by enabling control over the propagation environment by recycling EM signals. The recent developments in physics of meta-surfaces [4] may contribute to cost effective implementation of IRS-aided wireless systems. Thus, by intelligently controlling the phase-shifts introduced by the reflecting elements, the IRS-aided system can potentially overcome unfavorable propagation conditions, increase the coverage area while retaining a higher energy efficiency due to the passive reflecting elements.

A. Related Prior Research on Intelligent Reflecting Surfaces

In [2]–[4], [6], [7], the initial designs and theoretical modeling aspects of IRS-aided wireless communication are investigated. To this end, reference [2] explores the core architectural designs and features of IRS-based wireless communications. In [3], a new communication-theoretic model for the analysis and optimization of IRS-aided smart radio environments is proposed. In [4], prototypes of meta-surfaces and meta-tiles that can be used to coat objects embedded within a smart wireless propagation environment are already developed. In [6], the ray-tracing techniques are used to design novel propagation/path-loss models for IRS-aided wireless communications.

In [7], the path-loss models for IRS channels are designed based on the EM properties, and, these models are categorized into far-field, near-field beamforming, and near-field broadcasting.

References [8]–[15] provide performance analyses for IRS-enabled networks. Specifically, in [9], the fundamental performance metrics of IRS-aided communication systems operating over Rayleigh fading are derived. In [8], novel IRS-aided techniques are explored to boost the physical layer security aspects of wireless communications. In [10], the potential of the large intelligent surface (LIS)-aided communication in boosting the performance is investigated. Reference [11] explores the feasibility of exploiting statistical channel state information (CSI) to optimize phase-shift designs at the IRS to maximize the achievable spectral efficiency. In [12], the asymptotically achievable uplink sum rate of an IRS-aided system is analyzed by deriving the rate distributions for Rician fading channels. In [13], the impact of practically-viable/limited IRS control channels is investigated, and a passive beamformer design, which can achieve the asymptotic optimal received SNR under discrete reflection phase-shifts, is presented. In [13], a resource allocation algorithm to maximize the asymptotic sum rate under the passive beamforming is proposed. In [14], a performance comparison between the spherical and two-dimensional (2D) LIS deployments is presented, and it is shown that former can provide wider coverage while having simpler positioning and flexible implementation over the 2D counterpart. In [15], an analytical framework for random rotation based IRS-aided systems is presented, and four low-complexity schemes via selection-based and coding-based approaches are proposed.

In [16]–[23], the optimization-based algorithm designs are developed to intelligently control the phases of passive reflecting elements of an IRS to enable a myriad of wireless communication applications. In [16], [17], the joint optimization of precoders at the base-station (BS) and phase-shifts at the IRS is investigated, and the proposed solutions are based on the semidefinite relaxation and alternating optimization techniques. Reference [18] presents two computationally efficient algorithms to maximize the energy efficiency for the transmit power allocation based on alternating maximization adopting gradient descent method and sequential fractional programming approach. In [19], the beamforming designs are investigated with a practical phase-shift at the IRS. In [20], the capacity regions of the IRS-aided two user multiple-access channel are characterized. Thereby, the algorithms to find the inner and outer bounds of the capacity region are proposed for a centralized IRS deployment. Reference [21] investigates an IRS-aided wireless system operating in Rician fading channels by adopting maximal ratio transmission (MRT) at the BS. In [22], the joint optimization of active transmit and passive reflect beamforming is

investigated to maximize the secrecy rate for an IRS-aided secure communication system. In [23], the impact of artificial noise on IRS-aided secure communication is investigated.

In [24], a low-complexity passive reflective beamforming design is proposed for a multiple-input single-output system having distributed IRSs. By exploiting the statistical CSI, the achievable rate of the proposed system is analyzed. Reference [25] studies IRS selection and beam-routing for multiple IRSs-aided MIMO systems by maximizing the received signal powers at users through active and passive beamforming designs at the BS and IRSs, respectively. In [26], the concept of IRS selection and beam-routing in [25] is extended by adopting practical codebooks for optimizing active and passive beamforming. Authors in [27] propose two statistical distributions to approximate the channel distributions of two different dual-hop IRS-based wireless systems, namely, dual-hop IRS-aided scheme and IRS-aided transmit scheme. In [28], the asymptotic outage probability and the asymptotic sum rate are analyzed for a multiple IRSs-aided system over Rayleigh fading.

This paper goes well beyond our related conference paper [1] by presenting the average symbol error rate (SER), asymptotic outage/SER analysis in high SNR regime, diversity order, array/coding gain, achievable rate limits in large reflecting element regime, transmit power scaling laws, effects of transmission impairments of phase-shift quantization errors and correlated fading for the distributed IRSs-aided communication systems.

B. Motivation and Our Contribution

In this subsection, we explicitly highlight the motivation and distinct contribution of this work.

- 1) The main contribution of this work is to derive performance metrics for the distributed IRSs deployment over Nakagami- m fading in closed-form. The detrimental impacts of practical transmission impairments, including the phase-shift quantization errors and correlated fading, are investigated, and thereby, useful design insights are obtained through numerical results.
- 2) A common attribute of the above related prior works [6]–[21] is that their system models consist of a single IRS. However, the concept of IRS was originally envisioned to coat physical objects distributed within a wireless propagation channel. The fundamental performance metrics of a distributed IRSs-aided set-up have not yet been explored.
- 3) To fill this important gap in IRS literature, we present a statistical characterization of the end-to-end optimal SNR and the corresponding performance metrics of a distributed IRSs-

aided system over Nakagami- m fading. The optimal SNR is tightly approximated by using a mathematically tractable alternative through the central limit theorem (CLT) [29] because the optimal counterpart does not seem to be amenable to closed-form characterization of the performance metrics. Then, the probability density function (PDF) and cumulative distribution function (CDF) of this optimal SNR approximation are derived.

- 4) By using our PDF/CDF analysis, the outage probability, average SER, and achievable rate bounds/approximations are derived in closed-form. In order to obtain further insights, we resort to an asymptotic analysis of the outage probability and average SER in the high SNR regime through the first order polynomial expansions of the PDF of the corresponding random variables (RVs). Since we have not used the CLT approximation for our asymptotic analysis, our high SNR metrics are asymptotically accurate, and hence, they are used to quantify the achievable diversity order and array/coding gain in closed-form.
- 5) Our asymptotic analysis reveals that the achievable diversity order can be linearly increased with the product of the number of distributed IRSs and the number of elements in each IRS. Thus, diversity gains can also be achieved via passive reflections at the distributed IRSs deployment by recycling existing EM waves without generating additional EM waves by active RF chains. Our rate analysis in the large reflecting element regime reveals that our lower and upper bounds for the achievable rate are asymptotically accurate.
- 6) The impact of erroneously estimated phase-shifts is also quantified by adopting quantized phase-shifts at the IRSs. Moreover, the detrimental effect of spatial correlation at the reflecting elements is explored for the proposed distributed IRS set-up.
- 7) The accuracy of our analysis is verified via Monte-Carlo simulations, and a set of rigorous numerical results is presented to investigate the performance of the distributed IRSs. Our results reveal that a distributed deployment of IRSs can be exploited to boost the outage, average SER, and achievable rate performances compared to the direct transmission and single IRS-aided set-ups. We reveal that the practical transmission impairments such as phase-shift quantization errors and spatially correlated fading can hinder the performance gains. To this end, our analysis can be useful in quantifying the amount of performance degradation due to these practical impairments. Moreover, the performance gains of the distributed IRS set-up as compared to a single/large IRS with the same number of reflective elements depend on the locations of the IRSs.

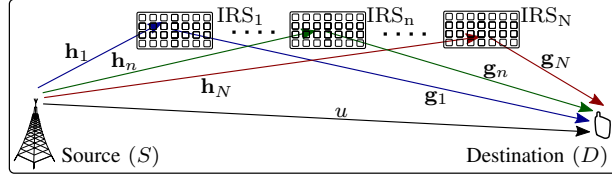


Fig. 1. System model - a distributed IRSs-aided communication set-up.

Notation: \mathbf{x}^T denotes the transpose of \mathbf{x} . $\mathbb{E}[X]$ and $\mathbb{V}\text{ar}[X]$ represent the expectation and variance of a RV X , respectively. $X \sim \mathcal{N}(\mu_X, \sigma_X^2)$ denotes that X is Gaussian distributed with μ_X mean and σ_X^2 variance. $\mathcal{O}(\cdot)$ denotes the higher order terms of the MacLaurin series expansion [30, Eq. (0.318.2)]. $\mathcal{Q}(\cdot)$ is the Gaussian- \mathcal{Q} function [29], $\Gamma(t)$ is the Gamma function [30, Eq. (8.310.1)], $\Gamma(\alpha, x)$ is the upper incomplete Gamma function [30, Eq. (8.350.2)], and $\gamma(\alpha, x)$ denotes the lower incomplete Gamma function [30, Eq. (8.350.1)]. Moreover, $\mathcal{K}_v(\cdot)$ represents the modified Bessel function of the second kind [30, Eq. (8.407)] and $F(\cdot, \cdot; \cdot; \cdot)$ is the Gauss Hypergeometric function [30, Eq. (9.100)]. Furthermore, $\text{mod}(\cdot, \cdot)$ denotes the modulo operator and $\lfloor \cdot \rfloor$ truncates the argument [31]

II. SYSTEM, CHANNEL AND SIGNAL MODELS

A. System and Channel Model

We consider a distributed IRSs-aided wireless system having a single-antenna source (S), a single-antenna destination (D), and N distributed IRSs with L passive reflective elements at each IRS (see Fig. 1). We assumed that S and D are placed in the far-field of the IRS. The S serves D through N distributed IRSs and via direct channel. It is assumed that the phase-shifts at the IRS reflective elements can be intelligently controlled such that the received signal at D can be constructively added by using an IRS controller, which connects the IRSs and the BS via a backhaul connection [16], [17]. The channels between S and the l th reflective element in the n th IRS and the l th reflective element in the n th IRS and D are denoted by h_{nl} and g_{nl} , respectively. Moreover, u denotes the direct channel between S and D . All channel envelopes are assumed to be independent Nakagami- m distributed, where m is the shape parameter. The direct channel (u) can be written in its polar form as

$$u = \alpha_u e^{j\theta_u}, \quad (1)$$

where α_u is the envelope of u and θ_u is the phase of u . The PDF of α_u is given by [29]

$$f_{\alpha_u}(x) = \frac{2m_u^{m_u} x^{2m_u-1}}{\Gamma(m_u) \xi_u^{m_u}} \exp\left(-\frac{m_u x^2}{\xi_u}\right), \quad (2)$$

where m_u is the shape parameter and $\xi_u = m_u \zeta_u$ is the scaling parameter. Here, ζ_u accounts for the large-scale fading/path-loss. The S -to-IRS and IRS-to- D channels can be defined as

$$v_{nl} = \alpha_{v_{nl}} e^{j\theta_{v_{nl}}}, \quad (3)$$

where $v \in \{h, g\}$, $\alpha_{v_{nl}}$ is the envelope of v_{nl} , and $\theta_{v_{nl}}$ is the phase. The PDF of $\alpha_{v_{nl}}$ is given as

$$f_{\alpha_{v_{nl}}}(x) = \frac{2m_v^{m_v} x^{2m_v-1}}{\Gamma(m_v) \xi_{v_n}^{m_v}} \exp\left(\frac{-m_v x^2}{\xi_{v_n}}\right), \quad (4)$$

where $m_{v_{nl}} = m_v$ and $\xi_{v_{nl}} = m_{v_{nl}} \zeta_{v_{nl}} = \xi_{v_n}$ are the shape and scaling parameters, respectively. It is assumed that large-scale fading parameters are the same for a given IRS because its reflective elements are co-located; $\xi_{v_{nl}} = \xi_{v_n}$, $\forall l$. However, ξ_{v_n} depends on the IRS index (n) because geographically distributed IRSs deployment.

B. Signal Model

The signal transmitted by S reaches at D through the reflected channels of N distributed IRSs and the direct channel. The signal received at D can be written as

$$r = \sqrt{P} \left(u + \sum_{n=1}^N \mathbf{g}_n^T \mathbf{\Theta}_n \mathbf{h}_n \right) x + w, \quad (5)$$

where x is the transmitted signal at S satisfying $\mathbb{E}[|x|^2] = 1$, P is the transmit power, and w is an additive white Gaussian noise (AWGN) at D having zero mean and variance of σ_w^2 such that $w \sim \mathcal{CN}(0, \sigma_w^2)$. In (5), $\mathbf{h}_n = [h_{n1}, \dots, h_{nl}, \dots, h_{nL}]^T \in \mathbb{C}^{L \times 1}$ is the channel vector between S and the n th IRS and $\mathbf{g}_n^T = [g_{n1}, \dots, g_{nl}, \dots, g_{nL}] \in \mathbb{C}^{1 \times L}$ accounts for the channel vector between the n th IRS and D . Moreover, $\mathbf{\Theta}_n = \text{diag}(\eta_{n1} e^{j\theta_{n1}}, \dots, \eta_{nl} e^{j\theta_{nl}}, \dots, \eta_{nL} e^{j\theta_{nL}}) \in \mathbb{C}^{L \times L}$ is a diagonal matrix, which captures the reflection properties of the n th IRS. Here, $\eta_{nl} e^{j\theta_{nl}}$ is a complex-valued reflection coefficient at the l th reflective element of the n th IRS, where η_{nl} and θ_{nl} are the magnitude of attenuation and phase-shift, respectively. Thus, the signal received at D in (5) can be rewritten as

$$r = \sqrt{P} \left(u + \sum_{n=1}^N \sum_{l=1}^L g_{nl} \eta_{nl} e^{j\theta_{nl}} h_{nl} \right) x + w. \quad (6)$$

The SNR at D can be derived via (6) as

$$\gamma = \bar{\gamma} \left| u + \sum_{n=1}^N \sum_{l=1}^L g_{nl} \eta_{nl} e^{j\theta_{nl}} h_{nl} \right|^2, \quad (7)$$

where $\bar{\gamma} = P/\sigma_w^2$ is the transmit SNR. Then, by substituting (1) and (3) into (7), this SNR can be written in terms of the channel phases as

$$\gamma = \bar{\gamma} \left| \alpha_u e^{j\theta_u} + \sum_{n=1}^N \sum_{l=1}^L \eta_{nl} \alpha_{g_{nl}} \alpha_{h_{nl}} e^{j(\theta_{nl} + \theta_{g_{nl}} + \theta_{h_{nl}})} \right|^2. \quad (8)$$

This analysis (8) reveals that the received SNR at D can be maximized when NL signal terms inside the summation of (8) are constructively added to the signal component received via the

direct channel. By controlling the phase-shifts at each IRS reflective element (θ_{nl}), the phases inside the double summation in (8) can be adjusted to enable a constructive addition of the received signal components via the direct and reflected channels. Thus, the optimal choice of θ_{nl} to maximize the received SNR at D can be given by [16]

$$\theta_{nl}^* = \underset{-\pi \leq \theta_{nl} \leq \pi}{\operatorname{argmax}} \gamma = \theta_u - (\theta_{g_{nl}} + \theta_{h_{nl}}), \quad (9)$$

for $n \in \{1, \dots, N\}$ and $l \in \{1, \dots, L\}$. By using (9), the optimal SNR at D can be derived as

$$\gamma^* = \bar{\gamma} \left[\alpha_u + \sum_{n=1}^N \sum_{l=1}^L \eta_{nl} \alpha_{g_{nl}} \alpha_{h_{nl}} \right]^2. \quad (10)$$

III. PRELIMINARY ANALYSIS

A. Statistical Characterization of the Optimal Received SNR

The $\alpha_{g_{nl}}$ and $\alpha_{h_{nl}}$ in (10) for $n \in \{1, \dots, N\}$ and $l \in \{1, \dots, L\}$ are independently distributed Nakagami RVs, and hence, the exact derivations of the PDFs of

$$Y = \sum_{n=1}^N \sum_{l=1}^L \eta_{nl} \alpha_{g_{nl}} \alpha_{h_{nl}}, \quad \text{and} \quad \gamma^* = \bar{\gamma} \underbrace{[\alpha_u + Y]^2}_R = \bar{\gamma} R^2, \quad (11)$$

seem mathematically involved and may not provide useful design insights. Nevertheless, even for moderately large values of the product NL , Y can be tightly approximated by an one-sided Gaussian distributed RV (\tilde{Y}) by invoking the CLT [29]. Then, an approximated PDF for Y can be written as (see Appendix A)

$$f_Y(y) \approx f_{\tilde{Y}}(y) = \frac{\psi}{\sqrt{2\pi\sigma_Y^2}} \exp\left(-\frac{(y - \mu_Y)^2}{2\sigma_Y^2}\right), \quad y \geq 0, \quad (12)$$

where $f_{\tilde{Y}}(y) = 0$ for $y < 0$, $\psi \triangleq 1/\mathcal{Q}(-\mu_Y/\sigma_Y)$ is a normalization factor to satisfy $\int_{-\infty}^{\infty} f_{\tilde{Y}}(x)dx = 1$.

In (12), μ_Y and σ_Y^2 can be derived via the moment matching technique as (see Appendix A)

$$\mu_Y = \sum_{n=1}^N \sum_{l=1}^L \eta_{nl} \sqrt{\frac{\xi_{h_n} \xi_{g_n}}{m_h m_g}} \frac{\Gamma(m_h + 1/2) \Gamma(m_g + 1/2)}{\Gamma(m_h) \Gamma(m_g)}, \quad (13a)$$

$$\sigma_Y^2 = \sum_{n=1}^N \sum_{l=1}^L \eta_{nl}^2 \left(\frac{\xi_{h_n} \xi_{g_n}}{m_h m_g} \right) \frac{\Gamma(m_h + 1) \Gamma(m_g + 1)}{\Gamma(m_h) \Gamma(m_g)} - \mu_Y^2. \quad (13b)$$

Then, a tight approximation of the PDF of R in (11) or the PDF of its approximation $\tilde{R} = \alpha_u + \tilde{Y}$ can be derived as (see Appendix B)

$$f_R(x) \approx f_{\tilde{R}}(x) = \lambda e^{-\Delta \left(\frac{x - \mu_Y}{2\sigma_Y^2 \sqrt{a}} \right)^2} \sum_{k=0}^{2m_u-1} \binom{2m_u-1}{k} \left(\frac{x - \mu_Y}{2\sigma_Y^2 \sqrt{a}} \right)^{2m_u-1-k} \left[\Gamma\left(\frac{k+1}{2}, \left(\frac{x - \mu_Y}{2\sigma_Y^2 \sqrt{a}} \right)^2 \right) \right]. \quad (14)$$

Here, a , λ , and Δ are given by

$$a = \frac{m_u}{\xi_u} + \frac{1}{2\sigma_Y^2}, \quad \text{and} \quad \lambda = \frac{m_u^{m_u} \psi}{\Gamma(m_u) \xi_u^{m_u} a^{m_u} \sqrt{2\pi\sigma_Y^2}}, \quad \text{and} \quad \Delta = \left(\frac{1}{2\sigma_Y^2} - \frac{1}{4a\sigma_Y^4} \right) 4\sigma_Y^4 a. \quad (15)$$

Via $\tilde{R} = \alpha_u + \tilde{Y}$ in (14), a tight approximation to the optimal SNR (γ^*) can be written as

$$\gamma^* \approx \tilde{\gamma}^* = \bar{\gamma} \tilde{R}^2. \quad (16)$$

Then, an approximation for the PDF of $\gamma^* = \bar{\gamma} R^2$ or the PDF of $\tilde{\gamma}^* = \bar{\gamma} \tilde{R}^2$ in (16) can be derived by using (14) as [29]

$$f_{\gamma^*}(y) \approx f_{\tilde{R}}\left(\sqrt{y/\bar{\gamma}}\right) / 2\sqrt{\bar{\gamma}y}. \quad (17)$$

Next, the CDF of \tilde{R} can be derived as (see Appendix C)

$$F_{\tilde{R}}(x) = 1 - \int_x^\infty f_{\tilde{R}}(u) du = 1 - \frac{\lambda}{2a^{m_u}} \sum_{k=0}^{2m_u-1} \binom{2m_u-1}{k} I_k, \quad (18)$$

where I_k is given as

$$I_k = \begin{cases} I_k^o, & \text{odd } k, \\ I_k^e, & \text{even } k. \end{cases} \quad (19)$$

In (19), I_k^o is given by

$$I_k^o = \begin{cases} \frac{q(\gamma_o-1)!}{2} \sum_{i=0}^{\gamma_o-1} \frac{(\Delta+1)^{\frac{k}{2}-m_u-i}}{i!} \left(2\Gamma\left(m_u+i+\frac{k}{2}\right) - \Gamma\left(m_u+i-\frac{k}{2}, (\Delta+1)l_{min}^2\right) \right), & \text{for } x < \mu_Y, \\ \frac{q(\gamma_o-1)!}{2} \sum_{i=0}^{\gamma_o-1} \frac{(\Delta+1)^{\frac{k}{2}-m_u-i}}{i!} \Gamma\left(m_u+i-\frac{k}{2}, (\Delta+1)l_{min}^2\right), & \text{for } x > \mu_Y, \end{cases} \quad (20)$$

where $q = 2\sigma_Y^2\sqrt{a}$, $\gamma_o = (k+1)/2$, and $l_{min} = (x - \mu_Y)/q$. Here, I_k^e in (19) can be given as

$$I_k^e = \frac{q(\gamma_e-1)!}{2} \sum_{j=0}^{\gamma_e-1} \frac{\Delta^{j-\gamma_e}}{j!} \left(\Gamma\left(\frac{k+1}{2}, l_{min}^2\right) l_{min}^{2j} e^{-\Delta l_{min}^2} - \frac{\Gamma\left(j+\frac{k}{2}+\frac{1}{2}, (\Delta+1)l_{min}^2\right)}{(\Delta+1)^{j+\frac{k}{2}+\frac{1}{2}}} \right), \quad (21)$$

where $\gamma_e = m - k/2$. Then, the CDF of $\gamma^* = \bar{\gamma} R^2$ can be approximated as [29]

$$F_{\gamma^*}(y) = \Pr(\gamma^* \leq y) \approx F_{\tilde{R}}\left(\sqrt{y/\bar{\gamma}}\right). \quad (22)$$

Remark 1: The accuracy of the approximated PDF and CDF of γ^* is verified by plotting (17), (22) and the Monte-Carlo simulations of the exact counterparts in Fig. 2. It reveals that our analytical approximations for the PDF (17) and CDF (22) of γ^* are accurate even for moderately large number of reflective elements (L) at the IRSs. Since IRSs are typically made of cost-effective reflective elements [32], a moderately large N is practically feasible.

IV. PERFORMANCE ANALYSIS

A. Outage Probability

The probability that the instantaneous SNR falls below a threshold SNR (γ_{th}) is defined as the SNR outage probability, and a tight approximation to it can be obtained from (22) as

$$P_{out} = P_r(\gamma \leq \gamma_{th}) \approx F_{\gamma^*}(\gamma_{th}). \quad (23)$$

This definition for P_{out} is used to quantify the asymptotic outage probability and the achievable diversity order in Section IV-D.

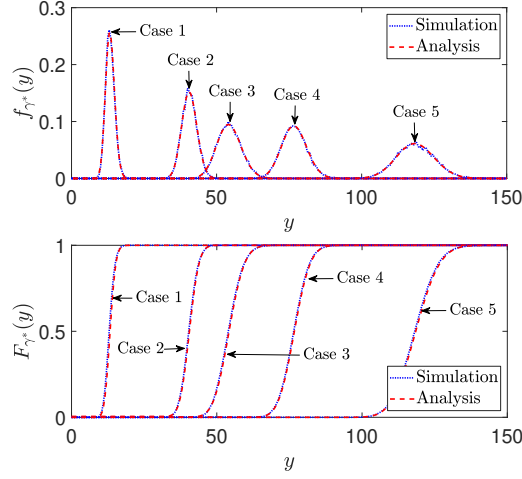


Fig. 2. The PDF and CDF of the received SNR (γ^*) for $\bar{\gamma} = -10\text{dB}$. The combinations of N and L for Case 1 to Case 5 are set to $\{N = 2, L = 32\}$, $\{N = 6, L = 32\}$, $\{N = 2, L = 64\}$, $\{N = 8, L = 32\}$, and $\{N = 2, L = 128\}$, respectively.

B. Average Achievable Rate

The average achievable rate can be defined as follows:

$$\mathcal{R} = \mathbb{E}[\log_2(1 + \gamma^*)]. \quad (24)$$

Since the exact derivation of \mathcal{R} in (24) seems mathematically intractable, we resort to tight upper and lower bounds by invoking the Jensen's inequality as [33]

$$\mathcal{R}_{lb} \leq \mathcal{R} \leq \mathcal{R}_{ub}. \quad (25)$$

In (25), \mathcal{R}_{lb} and \mathcal{R}_{ub} are defined as

$$\mathcal{R}_{lb} = \log_2(1 + (\mathbb{E}[1/\gamma^*])^{-1}) \approx \log_2(1 + (\mathbb{E}[1/\tilde{\gamma}^*])^{-1}), \quad (26a)$$

$$\mathcal{R}_{ub} = \log_2(1 + \mathbb{E}[\gamma^*]) \approx \log_2(1 + \mathbb{E}[\tilde{\gamma}^*]). \quad (26b)$$

The expectation term in (26b) can be approximately derived as (see Appendix D-A)

$$\mathbb{E}[\gamma^*] \approx \mathbb{E}[\tilde{\gamma}^*] = \bar{\gamma} (\sigma_u^2 + \sigma_Y^2 + 2\mu_u\mu_Y + \mu_u^2 + \mu_Y^2), \quad (27)$$

where μ_Y and σ_Y^2 are defined in (13a) and (13b), respectively. In (27), μ_u and σ_u^2 are defined as

$$\mu_u = \frac{\Gamma(m_u + 1/2)}{\Gamma(m_u)} \left(\frac{\xi_u}{m_u} \right)^{1/2}, \quad (28a)$$

$$\sigma_u^2 = \xi_u \left(1 - \frac{1}{m_u} \left(\frac{\Gamma(m_u + 1/2)}{\Gamma(m_u)} \right)^2 \right). \quad (28b)$$

Next, the expectation term in (26a) can be computed as

$$\mathbb{E}[1/\gamma^*] \approx \mathbb{E}[1/\tilde{\gamma}^*] = 1/\mathbb{E}[\tilde{\gamma}^*] + \text{Var}[\tilde{\gamma}^*]/(\mathbb{E}[\tilde{\gamma}^*])^3, \quad (29)$$

where $\mathbb{E}[\tilde{\gamma}^*]$ is defined in (27). Here, $\text{Var}[\tilde{\gamma}^*]$ is derived as (see Appendix D-B)

$$\text{Var}[\tilde{\gamma}^*] = \bar{\gamma}^2 \mathbb{E}[\tilde{R}^4] - (\mathbb{E}[\tilde{\gamma}^*])^2, \quad (30)$$

where $\mathbb{E}[\tilde{R}^4]$ is given by

$$\mathbb{E}[\tilde{R}^4] = \sum_{n=0}^4 \binom{4}{n} \mathbb{E}[\alpha_u^{(4-n)}] \mathbb{E}[\tilde{Y}^n]. \quad (31)$$

Here, $\mathbb{E}[\alpha_u^n]$ for $n \in \{1, 2, 3, 4\}$ can be derived as

$$\mathbb{E}[\alpha_u^n] = \frac{\Gamma(m_u + n/2)}{\Gamma(m_u)} \left(\frac{\xi_u}{m_u} \right)^{n/2}. \quad (32)$$

Moreover, $\mathbb{E}[\tilde{Y}^n]$ for $n \in \{1, 2, 3, 4\}$ is given by

$$\mathbb{E}[\tilde{Y}^n] = \frac{\psi}{2\sqrt{\pi}} \sum_{i=0}^n \binom{n}{i} \left(\sqrt{2\sigma_Y^2} \right)^{n-i} \mu_Y^i I\left(n-i, \frac{-\mu_Y}{2\sigma_Y^2}\right), \quad (33)$$

where $I(\cdot, \cdot)$ is given as

$$I(m, t) = \begin{cases} (-1)^m \gamma\left(\frac{m+1}{2}, t^2\right) + \Gamma\left(\frac{m+1}{2}\right), & \text{for } t \leq 0, \\ \Gamma\left(\frac{m+1}{2}, t^2\right), & \text{otherwise.} \end{cases} \quad (34)$$

Finally, \mathcal{R}_{lb} and \mathcal{R}_{ub} can be derived as

$$\mathcal{R}_{lb} = \log_2 \left(1 + \frac{\bar{\gamma} (\sigma_u^2 + \sigma_Y^2 + 2\mu_u \mu_Y + \mu_u^2 + \mu_Y^2)^3}{\sum_{n=0}^4 \binom{4}{n} \frac{\Gamma(m_u + (4-n)/2)}{\Gamma(m_u)} \left(\frac{\xi_u}{m_u} \right)^{(4-n)/2} \frac{\psi}{2\sqrt{\pi}} \sum_{i=0}^n \binom{n}{i} (2\sigma_Y^2)^{(n-i)/2} \mu_Y^i I\left(n-i, \frac{-\mu_Y}{2\sigma_Y^2}\right)} \right), \quad (35)$$

$$\mathcal{R}_{ub} = \log_2 \left(1 + \bar{\gamma} (\sigma_u^2 + \sigma_Y^2 + 2\mu_u \mu_Y + \mu_u^2 + \mu_Y^2) \right), \quad (36)$$

where μ_Y , σ_Y^2 , μ_u , and σ_u^2 are defined in (13a), (13b), (28a), and (28b), respectively.

1) *Asymptotic achievable rate as the number of IRS elements grows large ($L \rightarrow \infty$):* To obtain further insights, the asymptotic achievable rate can be derived as the number of IRS elements grows without bound ($L \rightarrow \infty$). In this operating regime, we observe that the transmit power can be scaled inversely proportional to the square of the number of IRS elements: $\lim_{L \rightarrow \infty} P = P_E/L^2$. By using this transmit power scaling law, the lower and upper rate bounds in (35) and (36), respectively, can be shown to approach an asymptotic limit as follows (see Appendix D-C):

$$\lim_{L \rightarrow \infty} \mathcal{R}_{lb} \longrightarrow \mathcal{R}^\infty, \quad \text{and} \quad \lim_{L \rightarrow \infty} \mathcal{R}_{ub} \longrightarrow \mathcal{R}^\infty, \quad (37)$$

where the asymptotic achievable rate \mathcal{R}^∞ in large L regime is given by

$$\lim_{L \rightarrow \infty} \mathcal{R} \longrightarrow \mathcal{R}^\infty = \log_2 \left(1 + \bar{\gamma}_E \left(\sum_{n=1}^N \eta_n \sqrt{\frac{\xi_{h_n} \xi_{g_n}}{m_h m_g}} \frac{\Gamma(m_h + 1/2) \Gamma(m_g + 1/2)}{\Gamma(m_h) \Gamma(m_g)} \right)^2 \right), \quad (38)$$

where $\bar{\gamma}_E = P_E/\sigma_w^2$ and $\eta_n = \eta_{nl}$, $\forall n$.

Remark 3: Our asymptotic analysis reveals that our lower (35) and upper (36) rate bounds converge to a common limit, and hence, these rate bounds are asymptotically accurate in large

L regime. Thus, a finite rate at D is achievable once the transmit power at S can be scaled inversely proportional to L^2 .

Remark 4: The physical dimension of a reflecting element is in the order of sub-wavelengths (i.e., $\lambda/10$ to $\lambda/5$, where λ is the wavelength) [34]. Thus, thousands of reflecting elements can be embedded in a relatively smaller surface area. To this end, the transmission distance differences of the channels from the furthest and closest elements of a given IRS to the destination can be assumed to be negligible in the far-field. Consequently, we assumed that the large-scale fading coefficients (η_{nl} for $l \in \{1, \dots, L\}$) are the same for a given IRS even for the asymptotic analysis in (38).

C. Average Symbol Error Rate (SER)

The average SER is the expectation of conditional error probability ($P_{e|\gamma^*}$) over the probability distribution of γ^* [35]. For a wide-range of coherent modulation schemes, $P_{e|\gamma^*}$ is given by [35]

$$P_{e|\gamma^*} = \omega \mathcal{Q} \left(\sqrt{\vartheta \gamma^*} \right), \quad (39)$$

where ω and ϑ depend on the modulation scheme [35]. For instance, the pair of parameters (ω, ϑ) for binary phase-shift keying (BPSK) and quadrature phase-shift keying (QPSK) are given by $(\omega = 1, \vartheta = 2)$ and $(\omega = 2, \vartheta = 1)$, respectively [35]. Then, the average SER can be defined as

$$\bar{P}_e = \mathbb{E} \left[\omega \mathcal{Q} \left(\sqrt{\vartheta \gamma^*} \right) \right]. \quad (40)$$

Then, by using $\tilde{\gamma}^*$ in (16), a tight approximation for the average SER can be derived as

$$\bar{P}_e \approx \tilde{P}_e = \omega \mathbb{E}_{\alpha_u} \left[\mathbb{E}_{\tilde{Y}} \left[\mathcal{Q} \left(\vartheta_b (\alpha_u + \tilde{Y}) \right) \right] \right], \quad (41)$$

where $\vartheta_b = \sqrt{\vartheta \gamma}$. A tight approximation to the average SER \tilde{P}_e is derived as (see Appendix E)

$$\tilde{P}_e \approx \omega B \sum_{k=0}^{2m_u-1} \left(\frac{-u_1}{2v_1} \right)^{2m_u-1-k} \Gamma(\gamma_b) \sum_{i=0}^{\gamma_b-1} \frac{v_1^{i-\gamma_b}}{i!} \left(\mathcal{Q}(\sqrt{2}r) \left(\frac{u_1}{2v_1} \right)^{2i} - \frac{s e^{\frac{u_2^2}{4v_2} - \frac{u_1^2}{4v_1} - r}}{\sqrt{\pi}} \sum_{j=0}^{2i} q_b^{2i-j} I_b \right), \quad (42)$$

where $\gamma_b = (k+1)/2$, $q_b = u_1/2v_1 - u_2/2v_2$, and I_b is defined as

$$I_b = \frac{v_2^{(j+1)/2}}{2} \begin{cases} \Gamma \left(\frac{j+1}{2}, \frac{u_2^2}{4v_2} \right), & \text{for } \frac{u_2}{2v_2} > 0, \\ (-1)^j \gamma \left(\frac{j+1}{2}, \frac{u_2^2}{4v_2} \right) + \Gamma \left(\frac{j+1}{2} \right), & \text{otherwise.} \end{cases} \quad (43)$$

Moreover, B , s , r , and $\{u_i, v_i\}$ for $i \in \{1, 2\}$ are defined as follows:

$$B = \frac{m_u^{m_u} \psi \exp \left(\frac{u_1^2}{4v_1} - \frac{\mu_Y^2}{2\sigma_Y^2} - \frac{1}{4a_1} \left(d\vartheta_b - \frac{\mu_Y}{\sigma_Y} \right)^2 \right)}{2\Gamma(m_u) \xi_u^{m_u} \sqrt{2\pi\sigma_Y^2 a_1}}, \quad \text{and} \quad s = \frac{c\vartheta_b^2}{2\sqrt{a_1}}, \quad (44a)$$

$$r = \frac{1}{2\sqrt{a_1}} \left(d\vartheta_b - \frac{\mu_Y}{\sigma_Y} \right), \quad \text{and} \quad u_1 = d\vartheta_b - \frac{c\vartheta_b^2}{a_1} \left(d\vartheta_b - \frac{\mu_Y}{\sigma_Y} \right), \quad (44b)$$

$$u_2 = u_1 + 2sr, \quad \text{and} \quad v_1 = c\vartheta_b - \frac{c^2\vartheta_b^2}{a_1} + \frac{m_u}{\xi_u}, \quad \text{and} \quad v_2 = v_1 + s^2, \quad (44c)$$

where $a_1 = c\vartheta_b^2 + 1/2\sigma_Y^2$, $c = 0.374$, and $d = 0.777$ [36].

D. Achievable Diversity Order

The diversity order is the negative slope of the average SER or outage probability versus the average SNR curve in a log-log scale in the high SNR regime [37], and it can be defined as

$$G_d = - \lim_{\bar{\gamma} \rightarrow \infty} \frac{\log(\bar{P}_e)}{\log(\bar{\gamma})} = - \lim_{\bar{\gamma} \rightarrow \infty} \frac{\log(P_{out})}{\log(\bar{\gamma})}. \quad (45)$$

The diversity order provides insights on how the outage probability or average SER decays with the average SNR. Thus, we derive the asymptotic outage probability and the average SER in the high SNR regime by using the first order polynomial expansion of the exact PDF of the corresponding RVs. The achievable diversity order and array/coding gain are also quantified. It is worth noting that our high SNR performance metrics are asymptotically accurate as we have not used CLT approximation for the corresponding derivations (see Appendix F). Thus, the achievable diversity order and array gains are accurate, and they are not approximated performance metrics.

1) *Asymptotic outage probability:* The outage probability can be asymptotically approximated in the high SNR regime as [37]

$$\lim_{\bar{\gamma} \rightarrow \infty} P_{out} = P_{out}^\infty \approx O_c \left(\frac{\gamma_{th}}{\bar{\gamma}} \right)^{G_d} + \mathcal{O}(\bar{\gamma}^{-(G_d+1)}), \quad (46)$$

where O_c is a measure of the array/coding gain and G_d is the diversity order [37]. Then, an asymptotic approximation for P_{out} can be derived as (see Appendix F)

$$P_{out}^\infty = \Omega \Phi(N, L) \left(\frac{\gamma_{th}}{\bar{\gamma}} \right)^{G_d} + \mathcal{O}(\bar{\gamma}^{-(G_d+1)}), \quad (47)$$

where the diversity order (G_d) is given by

$$G_d = NL \min(m_h, m_g) + m_u. \quad (48)$$

Moreover, in (47), Ω and $\Phi(N, L)$ are defined as

$$\Omega = \frac{m_u^{m_u} \Gamma(2m_u)}{G_d \Gamma(m_u) \xi_u^{m_u} \Gamma(2G_d)}, \quad \text{and} \quad \Phi(N, L) = \prod_{n=1}^N \prod_{l=1}^L \eta_{nl} \theta_n, \quad (49)$$

where $m_l = \max(m_h, m_g)$, $m_s = \min(m_h, m_g)$, and

$$\theta_n = \alpha' \sqrt{\pi} \left(4 \sqrt{\frac{m_s m_l}{\xi_{s_n} \xi_{l_n}}} \right)^{(m_s - m_l)} \begin{cases} \frac{|\ln(\epsilon)| \Gamma(2m_s + 1/2)}{\sqrt{\pi} \Gamma(2m_s)}, & \text{for } m_s = m_l, \\ \frac{\Gamma(2m_s) \Gamma(2m_l - 2m_s)}{\Gamma(m_l - m_s + 1/2)}, & \text{otherwise,} \end{cases} \quad (50a)$$

$$\alpha' = \frac{4}{\Gamma(m_s) \Gamma(m_l)} \left(\frac{m_s m_l}{\xi_{s_n} \xi_{l_n}} \right)^{(m_s + m_l)/2}. \quad (50b)$$

Furthermore, ξ_{s_n} and ξ_{l_n} are the scaling parameters related to m_s and m_l , respectively, in the Nakagami- m fading channels, and $1 \ll \epsilon < 0$ such that $\lim_{z \rightarrow 1^-} 1 - z$. Finally, O_c in (46) can be defined as

$$O_c = \Omega \Phi(N, L). \quad (51)$$

2) *Asymptotic average SER*: Similarly, the average SER can be approximated in the high SNR regime as [37]

$$\lim_{\bar{\gamma} \rightarrow \infty} \bar{P}_e = \bar{P}_e^\infty \approx (G_a \bar{\gamma})^{-G_d} + \mathcal{O}(\bar{\gamma}^{-(G_d+1)}), \quad (52)$$

where G_d and G_a are diversity order and array gain, respectively. An asymptotic approximation for the average SER (41) in high SNR regime can be derived as (see Appendix F)

$$\bar{P}_e^\infty = \left[(\Lambda \Phi(N, L))^{-\frac{1}{G_d}} \bar{\gamma} \right]^{-G_d} + \mathcal{O}(\bar{\gamma}^{-(G_d+1)}), \quad (53)$$

where $G_d = m_s N L + m_u$ and $\Phi(N, L)$ is given in (49). Moreover, Λ is defined as

$$\Lambda = \frac{\omega 2^{G_d-1} m_u^{m_u}}{\sqrt{\pi} \vartheta^{G_d} G_d \xi_u^{m_u}} \frac{\Gamma(G_d + 1/2) \Gamma(2m_u)}{\Gamma(2G_d) \Gamma(m_u)}. \quad (54)$$

Lastly, the array gain in (52) can be derived as

$$G_a = (\Lambda \Phi(N, L))^{-1/G_d}. \quad (55)$$

Remark 5: Our asymptotic performance analysis (48) reveals that the diversity order is a linear function of the number of distributed IRSs, the number of passive reflective elements in each IRS, and the m parameters of the Nakagami fading channels. It is worth noting that S and D are equipped with a single antenna/RF chain. However, as per analysis, we observe that the distributed IRSs deployment can be used to recycle the existing EM waves in the propagation environment without using additional active RF chains to substantially increase the diversity order, and consequently, the system reliability can be boosted in terms of lowering the outage probability and average SER. It is worth noting that the current state-of-the-art wireless systems, the diversity order improvements are obtained by virtue of increasing active RF chains and antennas at the transmitter/receiver.

Remark 6: By varying m parameter of Nakagami fading, a myriad of fading environments can be investigated. For instance, higher the m value, lesser the fading severity. The diversity order of a single reflected path corresponding to an IRS depends on the minimum value of Nakagami- m parameter of S -to-IRS and IRS-to- D channels. Thus, more severe channel (or equivalently, the channel with lesser m value) always determines the diversity order of a single IRS-aided reflected channel. However, when there exist distributed IRSs and a direct channel, the overall diversity order is the sum of the diversity orders of each end-to-end serviceable channel as per (48). The proposed distributed IRSs-aided system achieves this diversity gain by intelligently controlling the phase-shifts at the distributed passive reflective elements such that the signals received via reflected channels are constructively combined with the direct channel at D .

V. THE DETRIMENTAL EFFECTS OF TRANSMISSION IMPAIRMENTS

A. Effect of Phase Quantization Errors

Continuous phase-shift adjustments at the passive reflecting elements of the IRSs can be practically infeasible due to hardware limitations. Thus, we investigate the effect of erroneous phase-shifts at the IRSs by adopting a discrete phase-shift model to capture quantized phases. To this end, the IRS controller is allowed to select a discrete phase-shift for each reflecting element from a limited number of quantized phases. Thus, the selected discrete quantized phase for the l th reflective element in the n th IRS can be defined as

$$\hat{\theta}_{nl}^* = \pi\varsigma/2^{B-1}, \quad \text{for } l \in \{1, \dots, L\} \quad \text{and} \quad n \in \{1, \dots, N\}, \quad (56)$$

where B is the number of quantization bits. Moreover, ς is defined as

$$\varsigma = \underset{q \in \{0, \pm 1, \dots, \pm 2^{B-1}\}}{\operatorname{argmax}} |\theta_{nl}^* - \pi q/2^{B-1}|, \quad (57)$$

where θ_{nl}^* is optimal phase-shift given in (9). Then, the error in continuous and quantized phase-shifts can be defined as $\varepsilon_{nl} = \theta_{nl}^* - \hat{\theta}_{nl}^*$, which can shown to be uniformly distributed in the regime of large quantization levels as $\varepsilon_n \sim \mathcal{U}[-\tau, \tau)$, where $\tau = \pi/2^B$ [38]. Thus, we rewrite the optimal SNR given in (10) with quantized phase-shifts as follows:

$$\gamma^* = \bar{\gamma} \left| \alpha_u + \sum_{n=1}^N \sum_{l=1}^L \eta_{nl} \alpha_{g_{nl}} \alpha_{h_{nl}} e^{j\varepsilon_{nl}} \right|^2 = \bar{\gamma} [(\alpha_u + Y_R)^2 + Y_I^2], \quad (58)$$

where $Y_R = \sum_{n=1}^N \sum_{l=1}^L \eta_{nl} \alpha_{g_{nl}} \alpha_{h_{nl}} \cos(\varepsilon_{nl})$ and $Y_I = \sum_{n=1}^N \sum_{l=1}^L \eta_{nl} \alpha_{g_{nl}} \alpha_{h_{nl}} \sin(\varepsilon_{nl})$. Then, we can derive an upper bound for the average achievable rate with quantized phase-shifts by following the derivation steps similar to those in Appendix D as

$$\hat{\mathcal{R}}_{ub} = \log_2 \left(1 + \bar{\gamma} (\sigma_u^2 + \sigma_{Y_R}^2 + \sigma_{Y_I}^2 + 2\mu_u \mu_{Y_R} + \mu_u^2 + \mu_{Y_R}^2) \right), \quad (59)$$

where μ_u and σ_u^2 are given in (28a) and (28b), respectively. Moreover, μ_{Y_R} , $\sigma_{Y_R}^2$, and $\sigma_{Y_I}^2$ are defined as

$$\mu_{Y_R} = \sum_{n=1}^N \sum_{l=1}^L \eta_{nl} \sqrt{\frac{\xi_{h_n} \xi_{g_n}}{m_h m_g}} \frac{\Gamma(m_h + 1/2) \Gamma(m_g + 1/2)}{\Gamma(m_h) \Gamma(m_g)} \frac{\sin(\tau)}{\tau}, \quad (60a)$$

$$\sigma_{Y_R}^2 = \sum_{n=1}^N \sum_{l=1}^L \eta_{nl}^2 \frac{\xi_{h_n} \xi_{g_n}}{m_h m_g} \left[\frac{\Gamma(m_h + 1) \Gamma(m_g + 1)}{\Gamma(m_h) \Gamma(m_g)} \left(\frac{\sin(2\tau)}{4\tau} + \frac{1}{2} \right) - \left(\frac{\Gamma(m_h + \frac{1}{2}) \Gamma(m_g + \frac{1}{2}) \sin(\tau)}{\Gamma(m_h) \Gamma(m_g) \tau} \right)^2 \right], \quad (60b)$$

$$\sigma_{Y_I}^2 = \sum_{n=1}^N \sum_{l=1}^L \eta_{nl}^2 \frac{\xi_{h_n} \xi_{g_n}}{m_h m_g} \frac{\Gamma(m_h + 1) \Gamma(m_g + 1)}{\Gamma(m_h) \Gamma(m_g)} \left(\frac{1}{2} - \frac{\sin(2\tau)}{4\tau} \right). \quad (60c)$$

Remark 7: In an IRS-aided communication system, the imperfectly estimated cascaded channels result in imperfect phase-shift adjustments at the reflective elements [39]. Thus, the effects

of imperfectly estimated channels can be modeled as phase-shift errors, which are randomly distributed on $[-\pi, \pi)$ based on a certain circular distribution [39]. Hence, our analysis on phase quantization errors can be extended to capture the impacts of imperfect channel estimation of the proposed distributed IRS-aided wireless system.

B. Effect of Spatially-Correlated Fading

To capture deleterious effect of correlated fading for the reflecting elements at the IRSs, we consider a two-dimensional rectangular IRS having $L = L_H \times L_V$ elements, where L_H and L_V are the numbers of elements per row and column, respectively [40]. Moreover, we assume that each reflective element has an area of $A = d_H \times d_V$, where d_H is the horizontal width and d_V is the vertical height. Then, the correlation matrix at the n th IRS can be modeled as $\mathbf{R}_{v_n} \in \mathbb{C}^{L \times L}$ for $v \in \{h, g\}$, where the (i, j) th element of \mathbf{R}_{v_n} is given by [31]

$$[\mathbf{R}_{v_n}]_{i,j} = A \text{sinc}(2\|\mathbf{u}_{v_n,i} - \mathbf{u}_{v_n,j}\|/\lambda), \quad (61)$$

where λ is the wavelength of the plane wave, and $\mathbf{u}_{v_n,k}$ for $k \in \{i, j\}$ is defined as

$$\mathbf{u}_{v_n,k} = [0, \quad \text{mod}(k-1, L_H)d_H, \quad \lfloor (k-1)/L_H \rfloor d_V]^T. \quad (62)$$

When there exists correlated fading, S -nth IRS and n th IRS- D channels can be modeled as

$$\tilde{\mathbf{h}}_n = \mathbf{R}_{h_n}^{1/2} \mathbf{h}_n, \quad \text{and} \quad \tilde{\mathbf{g}}_n^T = \mathbf{g}_n^T \mathbf{R}_{g_n}^{1/2}, \quad (63)$$

where $\mathbf{h}_n = [h_{n1}, \dots, h_{nl}, \dots, h_{nL}]^T \in \mathbb{C}^{L \times 1}$ and $\mathbf{g}_n^T = [g_{n1}, \dots, g_{nl}, \dots, g_{nL}] \in \mathbb{C}^{1 \times L}$. Then, the SNR at D can be written as

$$\gamma = \bar{\gamma} \left| u + \sum_{n=1}^N \tilde{\mathbf{g}}_n^T \Theta_n \tilde{\mathbf{h}}_n \right|^2 = \bar{\gamma} \left| \alpha_u e^{j\theta_u} + \sum_{n=1}^N \mathbf{g}_n^T \mathbf{R}_{g_n}^{1/2} \Theta_n \mathbf{R}_{h_n}^{1/2} \mathbf{h}_n \right|^2. \quad (64)$$

In the presence of spatially correlated fading, the SNR in (64) can be maximized by considering the phases introduced by correlation matrices. To this end, the optimal choice of θ_{nl} to maximize the received SNR at D can be given by

$$\theta_{nl}^* = \theta_u - \left(\tilde{\theta}_{g_{nl}} + \tilde{\theta}_{h_{nl}} \right), \quad \text{for } n \in \{1, \dots, N\} \quad \text{and} \quad l \in \{1, \dots, L\}, \quad (65)$$

where $\tilde{\theta}_{h_{nl}}$ and $\tilde{\theta}_{g_{nl}}$ are phases of $[\tilde{\mathbf{h}}_n]_{l,1}$ and $[\tilde{\mathbf{g}}_n^T]_{1,l}$, respectively, which account for the cumulative phases of the corresponding correlation matrices and independently faded channels. Thereby, the average achievable rate for the distributed IRS set-up with correlated fading can be written as

$$\mathcal{R} = \mathbb{E} \left[\log_2 \left(1 + \bar{\gamma} \left| \alpha_u + \sum_{n=1}^N \hat{\mathbf{g}}_n^T \boldsymbol{\eta}_n \hat{\mathbf{h}}_n \right|^2 \right) \right], \quad (66)$$

where $\boldsymbol{\eta}_n = \text{diag}(\eta_{n1}, \dots, \eta_{nl}, \dots, \eta_{nL}) \in \mathbb{C}^{L \times L}$. Moreover, $\hat{\mathbf{h}}_n$ and $\hat{\mathbf{g}}_n$ represent the vectors with the moduli of the elements of $\tilde{\mathbf{h}}_n$ and $\tilde{\mathbf{g}}_n$, respectively.

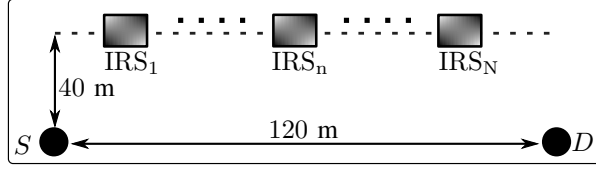


Fig. 3. The simulation set-up of the distributed IRSs-aided communication system.

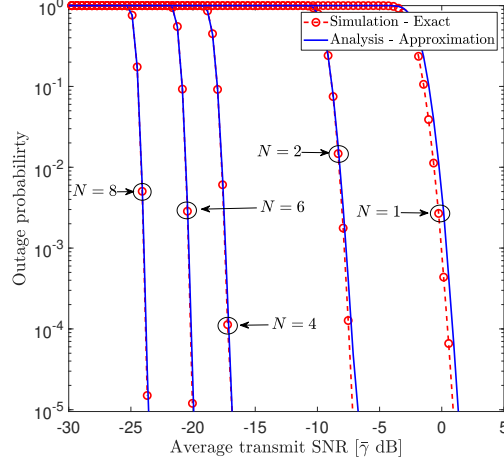


Fig. 4. The outage probability for different number of IRSs in the distributed deployment denoted by $N \in \{1, 2, 4, 6, 8\}$, the number of reflective elements per IRS is $L = 32$, $m_u = m_h = m_g = 3$, the threshold SNR is $\gamma_{th} = 0$ dB.

VI. NUMERICAL RESULTS

In this section, we present our numerical results to investigate the performance gains and to validate our analysis. We consider the simulation set-up in Fig. 3, where S and D are in positioned at fixed locations and 120 m apart from each other. Unless otherwise specified, the IRSs are uniformly deployed in between S and D such that the minimum distance between S or D and the closest IRS is greater the 40 m. The large-scale fading is modeled as $\zeta_{ab} = (d_0/d_{ab})^\nu \times 10^{\varphi_{ab}/10}$, where $a \in \{S, n\}$, $b \in \{n, D\}$, d_{ab} is the distance between nodes a and b , $d_0 = 1$ m is a reference distance, $\nu = 2.8$ is the path-loss exponent, and $10^{\varphi_{ab}/10}$ captures log-normal shadow fading with $\varphi_{ab} \sim \mathcal{N}(0, 8)$ [41]. Moreover, the amplitude of reflection coefficients η_{nl} for $n \in \{1, \dots, N\}$ and $l \in \{1, \dots, L\}$ is set to 0.9, and unless otherwise specified, the Nakagami- m parameters (m_u , m_h , and m_g) are set to 3.

In Fig. 4, we plot the outage probability as a function of the average transmit SNR ($\bar{\gamma}$) by varying the number of distributed IRSs defined by $N \in \{1, 2, 4, 6, 8\}$. The exact outage curves are generated by using Monte-Carlo simulation, while the analytical outage curves are plotted via our closed-form derivation in (23). As per Fig. 4, we observe that the tightness of our outage probability approximation significantly improves with N . Moreover, we observe that the distributed IRSs deployment outperforms the single-IRS set-up. For example, the single-IRS

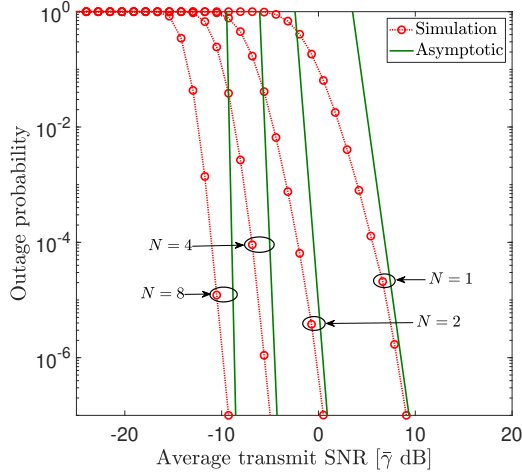


Fig. 5. The outage probability for $N \in \{1, 2, 4, 8\}$, $L = 6$, $m_u = m_g = 3$, $m_h = 1.5$, and $\gamma_{th} = 10$ dB.

deployment requires an average transmit SNR of 1 dB to achieve an outage probability of 10^{-4} , and this is an 104.2% increase compared to the same transmit SNR requirement of the distributed deployment with eight IRSs.

In Fig. 5, we investigate asymptotic behavior of the outage probability in the high SNR regime. To this end, our asymptotic outage probability (47) is plotted as a function of the average transmit SNR, and Monte-Carlo simulations are also provided for validation purposes. The asymptotic outage probability curves reveal the achievable diversity orders for different distributed IRSs deployments; $N \in \{1, 2, 4, 8\}$. For instance, the diversity orders for $(N = 1, L = 6)$ and $(N = 2, L = 6)$ cases can be obtained by computing the negative gradients of asymptotic outage curves in Fig. 5 to be 12 and 21, respectively. This observation clearly validates our diversity order analysis in (48), i.e., $G_d = NL \min(m_h, m_g) + m_u$ with $m_h = 1.5$, $m_g = m_u = 3$. Thus, the results in Fig. 5 show that the diversity order increases with the number of IRS reflective elements, and consequently, the system reliability can be drastically improved by the proposed distributed IRSs-aided system without adopting additional RF chains.

In Fig. 6, we plot the achievable average rate for different number of distributed IRSs as per $N \in \{1, 2, 4, 6, 8\}$. The achievable rate lower/upper bounds are plotted via (26a) and (26b), respectively. The accuracy of our rate analysis is also validated via Monte-Carlo simulation of the exact achievable rate. Fig. 6 clearly depicts that our lower/upper bounds are tight even for smaller N . Fig. 6 reveals that higher the number of distributed IRSs, higher the achievable rate. Moreover, Fig. 6 can be used to quantify the rate gains of the distributed IRSs deployment compared to the direct transmission. For instance, the single-IRS ($N = 1$) case provides a rate

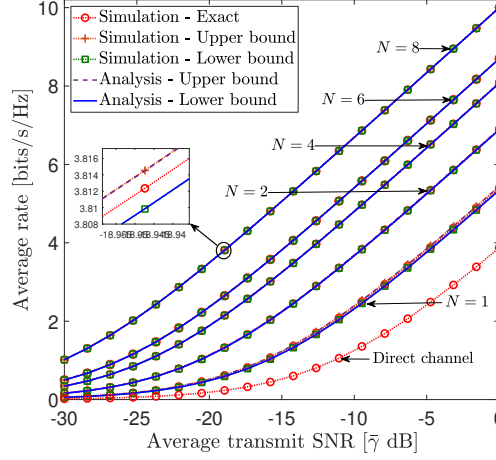


Fig. 6. The average achievable rate for $N \in \{1, 2, 4, 6, 8\}$, $L = 32$, and $m_u = m_h = m_g = 3$.

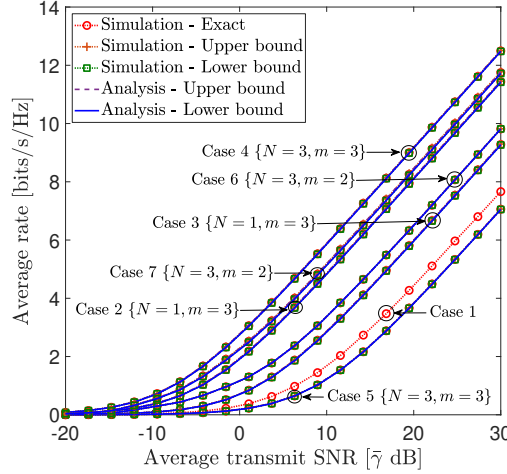


Fig. 7. An average achievable rate comparison for different system configurations. For all cases $L = 32$ and $m_u = m_h = m_g = m$. The cases are defined as follows: Case-1: direct channel only, Case-2/Case-3: IRSs are located in closer with/without direct channel, Case-4/Case-6/Case-7: IRSs are located far-away and with direct channel, and Case-5: IRSs are located far-away and without direct channel, respectively.

gain of 80.7% compared to the direct transmission at an average transmit SNR of -10 dB. This rate gain increases to 182.5%, 266.2%, and 405.9% for dual-, quadruple-, and octuple-IRS cases, respectively, with respect to the direct channel.

In Fig. 7, the effects of the IRS positions and the shape parameter (m) of the Nakagami fading are investigated. To this end, S and D are positioned at fixed locations at 50 m apart. The Case-1 plots the achievable rate of the direct channel. For Case-2 and Case-3, the distances between S -IRS and D -IRS are 75 m. Moreover, the distances between S -IRS and D -IRS for Case-4 to Case-7 are greater than 160 m. In Case-3 and Case-5, the achievable rates are plotted by assuming that the direct channel is not serviceable, and the end-to-end communication is established via the reflected channels. Fig. 7 shows that the rate of the direct channel is higher

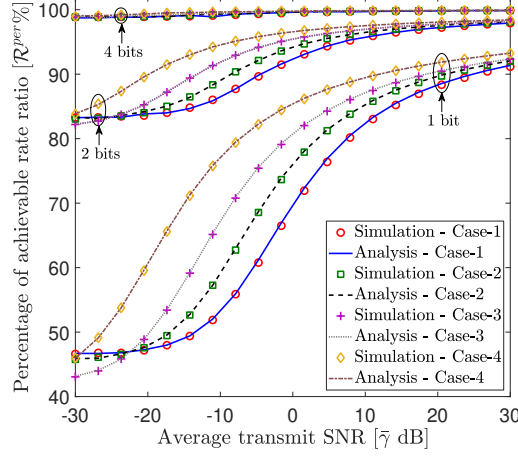


Fig. 8. The impact of phase-shift quantization errors on the achievable rate for $N \in \{1, 2, 4, 6\}$, $L = 32$, and $m_u = m_h = m_g = 3$.

than that of the reflected channels when the IRSs are positioned far away from S and D (see Case-1 and Case-5). When comparing Case-2 and Case-3, we can observe that having the direct channel is beneficial in boosting the achievable rate. Although the IRSs are placed far away in Case-4 than that in Case-3, the achievable rate of the former is higher than that of the latter. This is because Case-4 has two additional IRSs than the Case-3. Thus, the distributed IRSs deployment can circumvent the rate losses incurred due to larger transmission distances in the reflected channels. Moreover, Case-6 and Case-7 show the impact of different m parameter of Nakagami fading. In Case-6, $m = 1$ leads to have Rayleigh fading channel, whereas in Case-7, $m = 2$ depicts the achievable rate of Rician fading with 1.5 dB Rician factor.

In Fig. 8, the effect of phase-shift quantization errors is studied for different number of IRSs ($N \in \{1, 2, 4, 6\}$) and distinct number of quantization bits ($B \in \{1, 2, 4\}$), by plotting the percentage rate ratio (\mathcal{R}^{per}) as a function of the average transmit SNR. The percentage rate ratio is defined as $\mathcal{R}^{per} = \hat{\mathcal{R}}_{ub} / \mathcal{R}_{ub} \times 100\%$, where \mathcal{R}_{ub} denotes the upper bound of the achievable rate with continuous phase-shifts in (36), while $\hat{\mathcal{R}}_{ub}$ is the average achievable rate upper bound with phase-shift quantization errors in (59). Monte-Carlo simulations are also plotted for the purpose of validating the analysis. From Fig. 8, we observe that the effect of phase-shift quantization errors can be neglected when a higher number of quantization levels is adopted. For example, compared to the continuous phase-shifts, 99% of the average achievable rate can be recovered with four-bit phase-shift quantization. Moreover, \mathcal{R}^{per} can be improved by employing a higher number of distributed IRSs. For instance, at an transmit SNR of 0 dB, $N = 2$ case provides a gain of percentage rate ratio of 8.0% compared to the single IRS case for one-bit quantization.

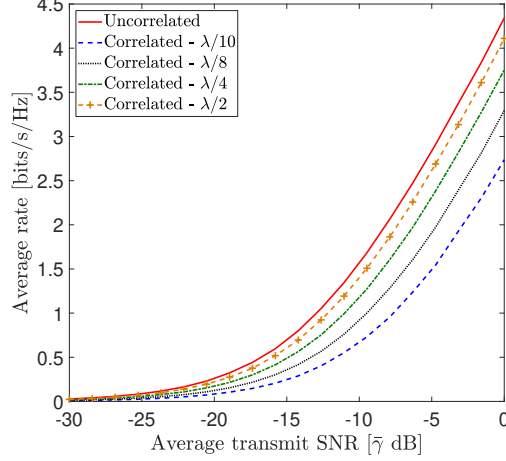


Fig. 9. The impact of correlated fading on the achievable rate for $N = 2$, $L = 64$, $m_u = m_h = m_g = 3$, and $d_H = d_V \in \{\lambda/2, \lambda/4, \lambda/8, \lambda/10\}$.

Furthermore, this percentage rate gain increases to 13.6% and 19.3% for $N = 4$ and $N = 6$ cases, respectively. Fig. 8 also depicts that the high transmit SNR is also beneficial for recovering the average achievable rate.

In Fig. 9, the effect of correlated fading is investigated by plotting the average achievable rate as a function of the average transmit SNR ($\bar{\gamma}$) for different sizes of passive reflectors as $d_H = d_V \in \{\lambda/2, \lambda/4, \lambda/8, \lambda/10\}$, respectively. The correlation model in (61) is adopted at each IRS for generating the correlated achievable rate curves, while uncorrelated achievable rate curves are plotted by setting $\mathbf{R}_{v_n} = \mathbf{I}_L$ for $v \in \{h, g\}$ and $n \in \{1, \dots, N\}$. Fig. 9 clearly shows that the spatially correlated fading detrimentally affects the achievable rate compared to the uncorrelated fading case. Since the correlation matrices are proportional to the area of reflecting elements (i.e., $\mathbf{R}_{v_n} \propto A$), the achievable rate increases with the size of reflecting elements at IRSs. Thus, the performance metrics for the uncorrelated fading may be used as upper bounds or benchmarks for practical implementations with smaller reflecting elements under spatial correlated fading cases.

In Fig. 10, the average bit error rate (BER) of BPSK is plotted against the average transmit SNR ($\bar{\gamma}$) for different number of IRSs; $N \in \{1, 2, 4, 6, 8\}$. The exact average BER curves are generated via Monte-Carlo simulations, where as the analytical curves are plotted by using (42). From Fig. 10, we observe that our average BER analysis in (42) is tight for moderately larger NL regime. The average BER for a single-IRS set-up is also plotted for the purpose of comparison. Fig. 10 reveals that the distributed IRSs deployment outperforms the single-IRS set-up. For instance, to achieve an average BER of 10^{-4} , the single-IRS set-up requires an average transmit

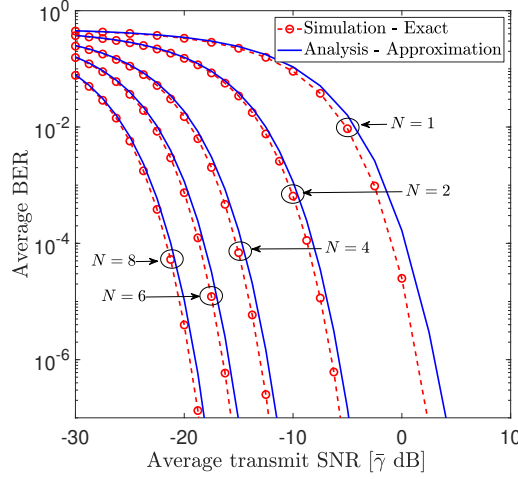


Fig. 10. The average BER of BPSK versus average transmit SNR ($\bar{\gamma}$) for $N \in \{1, 2, 4, 6, 8\}$, $L = 32$, $m_u = m_h = m_g = 3$, $\omega = 1$, and $\vartheta = 2$.

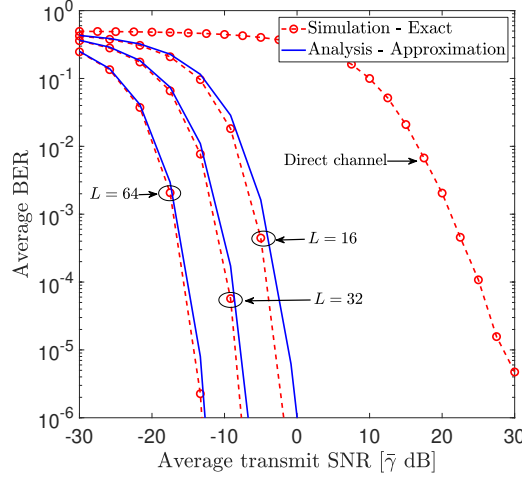


Fig. 11. A comparison of the average BER with/without IRSs for $N = 2$, $L \in \{16, 32, 64\}$, $m_u = m_h = m_g = 3$, $\omega = 1$, and $\vartheta = 2$.

SNR of 0 dB, which is an 22 dB increase compared to the transmit SNR requirement of the distributed IRSs set-up with eight IRSs. Moreover, the achievable average BER significantly decreases when the number of distributed IRSs grows large. For example, at an average SNR of -20 dB, the average BER of $N = 4$ case is lowered by 99.8% by doubling the number of IRSs to $N = 8$.

In Fig. 11, we investigate the effects of increasing number of IRS reflective elements by plotting the average BER of BPSK versus the average SNR. A dual-IRS system is considered and the number of reflective elements is varied as $L \in \{16, 32, 64\}$. Analytical average BER is plotted via (42), and it is validated through Monte-Carlo simulations. Fig. 11 shows that the dual-IRS system outperforms the direct channel in terms of the average BER. For example, the direct transmission requires an average SNR of 28 dB to achieve an average BER of 10^{-5} ,

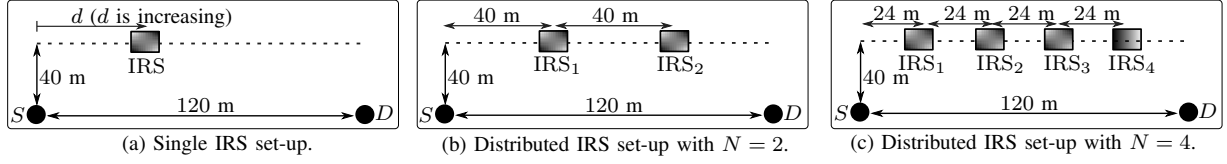


Fig. 12. The simulation set-ups for Fig. 13.

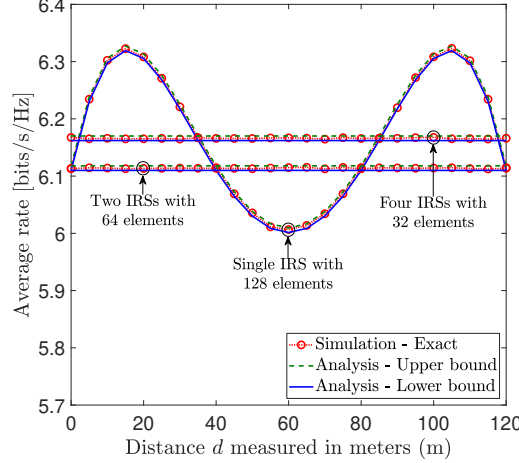


Fig. 13. The average achievable rate versus the distance for $N \in \{1, 2, 4\}$, $L = \{128, 64, 32\}$, $m_u = m_h = m_g = 3$, and $\bar{\gamma} = 0$ dB.

while this SNR requirement can be lowered by 36 dB with a deployment of a dual-IRS set-up with $L = 32$. Moreover, at an average SNR of -10 dB, the average BER can be lowered from 1.82×10^{-2} to 1.72×10^{-4} by doubling the number of reflective elements per IRS from $L = 16$ case to $L = 32$ case. Thus, the proposed distributed IRSs deployment can be used to significantly boost the reliability of wireless communication systems.

In Fig. 13, we compare the achievable rate performance of a single IRS with NL elements with N distributed IRSs with L elements. Our aim is to investigate the location regions in which a single IRS would outperform the distributed IRS set-ups in terms of the achievable rate. To this end, we consider three cases: (a) a single IRS case, where the position of the IRS (d) is varied between S and D (see Fig. 12-a), (b) two uniformly distributed IRSs with $L = 64$ (see Fig. 12-b), and (c) four uniformly distributed IRSs with $L = 32$ (see Fig. 12-c). In the distributed IRS cases, the locations of the IRSs are fixed and for all the cases, the product of the number of IRSs and the number of elements is kept at a fixed value $NL = 128$. We plot the average achievable rate with distance d . The achievable rates of the distributed IRS cases do not vary with d since the corresponding IRSs are kept at fixed locations as shown in Fig. 12-b and Fig. 12-c. However, since we change the position of the single IRS between S and D , its achievable rate varies with the distance d . From Fig. 13, we observe that there exist two distance regions in which the single

IRS set-up outperforms the distributed IRSs in terms of the achievable rate. For instance, when the single IRS is placed nearer to S or D , it achieves high achievable rates compared to that of the distributed IRS cases with fixed locations. On the other hand, when the location of the single IRS is in between $d = 40$ m and $d = 80$ m (which is around the midpoint ($d = 60$ m)), the both distributed IRS set-ups with $\{N = 2, L = 64\}$ and $\{N = 4, L = 32\}$ outperform the single IRS case in terms of the achievable rate. The observations of Fig. 13 clearly reveal that an optimally positioned single IRS with NL elements outperforms N uniformly distributed IRSs with each having L elements. Thus, the positioning of IRSs in a distributed set-up is a key factor in optimizing the performance gains.

VII. CONCLUSION

In this paper, the fundamental performance metrics of a distributed IRSs-aided communication system have been investigated. The optimal received SNR has been derived by controlling the phase-shifts of the distributed IRS elements. To facilitate a mathematically tractable performance analysis, this SNR has been statistically characterized by deriving the tight approximations to the PDF and CDF for Nakagami- m fading. Then, the outage probability, average SER, and achievable rate approximations/bounds have been derived. Useful insights on the diversity order and array gain have been drawn by deriving the asymptotic outage probability and the average SER in the high SNR regime. By virtue of an asymptotic rate analysis, it has been shown that the transmit power can be scaled inversely proportional to the square of the number of reflective elements, and in this operating regime, our lower and upper rate bounds have been shown to be asymptotically accurate. The detrimental effects of phase-shift quantization errors and spatially-correlated fading at the IRSs have been investigated for the proposed distributed IRSs set-up. A rigorous set of Monte-Carlo simulations has been presented to validate the accuracy of our analysis. The performance of the proposed distributed IRSs-aided set-up has been compared with a conventional/direct and a single IRS-aided counterparts. Our analysis and numerical results reveal that distributed IRSs deployment can be used to significantly enhance the performance of future wireless communications by recycling the existing EM waves via passive IRS reflective elements without generating new EM waves with active RF chains. Thus, the concept of distributed IRSs-aided communications can be an energy and cost effective paradigm-shift in future wireless designs.

APPENDIX A

THE DERIVATION OF μ_Y IN (13a), σ_Y^2 IN (13b), AND PDF OF Y IN (12)

First, we define $Y = \sum_{n=1}^N \sum_{l=1}^L \eta_{nl} z_{nl}$, where $z_{nl} = \alpha_{h_{nl}} \alpha_{g_{nl}}$. Since $\alpha_{h_{nl}}$ and $\alpha_{g_{nl}}$ are independent Nakagami- m RVs, the PDF of z_{nl} can be evaluated as

$$\begin{aligned} f_{z_{nl}}(x) &= \int_0^\infty f_{\alpha_{h_{nl}}}(u) f_{\alpha_{g_{nl}}}(x/u) \times \frac{1}{|u|} du = \alpha x^{2m_g-1} \int_0^\infty u^{2(m_h-m_g)-1} e^{-\frac{m_h u^2}{\xi_{h_n}} - \frac{m_g x^2}{\xi_{g_n} u^2}} du \\ &\stackrel{(a)}{=} \frac{\alpha}{2} x^{2m_g-1} \int_0^\infty t^{m_h-m_g-1} e^{-\frac{m_h t}{\xi_{h_n}} - \frac{m_g x^2}{\xi_{g_n} t}} dt \stackrel{(b)}{=} \alpha' x^{m_h+m_g-1} \mathcal{K}_{m_h-m_g} \left(2x \sqrt{\frac{m_h m_g}{\xi_{h_n} \xi_{g_n}}} \right), \end{aligned} \quad (67)$$

where $\alpha = 4m_h^{m_h} m_g^{m_g} / (\Gamma(m_h) \Gamma(m_g) \xi_{h_n}^{m_h} \xi_{g_n}^{m_g})$ and $\alpha' = \alpha (m_g \xi_{h_n} / m_h \xi_{g_n})^{\frac{m_h-m_g}{2}}$. The step (a) is obtained by letting $t = u^2$ and the step (b) is computed via [30, Eq. (3.471.9)]. Then, the n th moment of z_{nl} is derived as

$$\begin{aligned} \mathbb{E}[z_{nl}^n] &= \alpha' \int_0^\infty x^{m_h+m_g+n-1} \mathcal{K}_{m_h-m_g} \left(2x \sqrt{\frac{m_h m_g}{\xi_{h_n} \xi_{g_n}}} \right) dx \\ &\stackrel{(c)}{=} \frac{\alpha'}{4} \left(\frac{m_h m_g}{\xi_{h_n} \xi_{g_n}} \right)^{\frac{-m_h-m_g-n+1}{2}} \Gamma \left(\frac{2m_h+n}{2} \right) \Gamma \left(\frac{2m_g+n}{2} \right), \end{aligned} \quad (68)$$

where the step (c) is written via [30, Eq. (6.561.16)]. The mean and variance of Y are given as

$$\mu_Y = \mathbb{E}[Y] = \sum_{n=1}^N \sum_{l=1}^L \eta_{nl} \mathbb{E}[z_{nl}], \quad \text{and} \quad \sigma_Y^2 = \mathbb{V}\text{ar}[Y] = \sum_{n=1}^N \sum_{l=1}^L \eta_{nl}^2 (\mathbb{E}[z_{nl}^2] - \mathbb{E}[z_{nl}]^2). \quad (69)$$

By substituting (68) into (69), μ_Y and σ_Y^2 can be computed as (13a) and (13b), respectively. Then, the PDF of Y can be approximated by an one-sided Gaussian distribution as given in (12) by invoking the central limit theorem [29].

APPENDIX B

THE DERIVATION OF PDF OF \tilde{R} IN (14)

Since α_u and Y are independent RVs, the PDF of $\tilde{R} = \alpha_u + \tilde{Y}$ can be derived as follows:

$$\begin{aligned} f_{\tilde{R}}(x) &= \int_0^\infty f_u(u) f_{\tilde{Y}}(x-u) du = 2a^{m_u} \lambda e^{-\frac{(x-\mu_Y)^2}{2\sigma_Y^2}} \int_0^\infty u^{2m_u-1} e^{-au^2+bu} du \\ &= 2a^{m_u} \lambda e^{-\frac{(x-\mu_Y)^2}{2\sigma_Y^2}} e^{\frac{b^2}{4a}} \underbrace{\int_0^\infty u^{2m_u-1} e^{-a\left(u-\frac{b}{2\sqrt{a}}\right)^2} du}_{I_{\tilde{R}}}, \end{aligned} \quad (70)$$

where $b = (x - \mu_Y) / \sigma_Y^2$. Here, a and λ are defined in (15). The solution to $I_{\tilde{R}}$ in (70) is given by

$$\begin{aligned} I_{\tilde{R}} &= \frac{1}{a^{m_u}} \int_{\frac{-b}{2\sqrt{a}}}^\infty \left(t + \frac{b}{2\sqrt{a}} \right)^{2m_u-1} e^{-t^2} dt = \frac{1}{a^{m_u}} \sum_{k=0}^{2m_u-1} \binom{2m_u-1}{k} \left(\frac{b}{2\sqrt{a}} \right)^{2m_u-1-k} \int_{\frac{-b}{2\sqrt{a}}}^\infty t^k e^{-t^2} dt \\ &\stackrel{(d)}{=} \frac{1}{2a^{m_u}} \sum_{k=0}^{2m_u-1} \binom{2m_u-1}{k} \left(\frac{b}{2\sqrt{a}} \right)^{2m_u-1-k} \Gamma \left(\frac{k+1}{2}, \frac{b^2}{4a} \right), \end{aligned} \quad (71)$$

where the step (d) is due to [30, Eq. (2.33.10)]. By substituting (b) and (71) into (70), the PDF of \tilde{R} is derived as (14).

APPENDIX C
THE DERIVATION OF CDF OF \tilde{R} IN (18)

By substituting (14) into (18), I_k in (18) can be given as

$$I_k = \int_x^\infty e^{-\Delta \left(\frac{u-\mu_Y}{q}\right)^2} \left(\frac{u-\mu_Y}{q}\right)^{2m_u-1-k} \Gamma\left(\frac{k+1}{2}, \left(\frac{u-\mu_Y}{q}\right)^2\right) du$$

$$\stackrel{(e)}{=} q \int_{l_{min}}^\infty e^{-\Delta t^2} t^{2m_u-1-k} \Gamma\left(\frac{k+1}{2}, t^2\right) dt, \quad (72)$$

where $q = 2\sigma_Y^2\sqrt{a}$, $l_{min} = (x - \mu_Y)/q$, and the step (e) is written by changing the variable of integration. Then, we divide I_k into two integrals: (i) I_k^o for odd values of k and (ii) I_k^e for even values of k . Thus, for odd values of k and when $x - \mu_Y < 0$, this integral can be written as

$$I_k^o = q \underbrace{\int_{l_{min}}^0 e^{-\Delta t^2} t^{2m_u-1-k} \Gamma\left(\frac{k+1}{2}, t^2\right) dt}_{I_{k1}^o} + q \underbrace{\int_0^\infty e^{-\Delta t^2} t^{2m_u-1-k} \Gamma\left(\frac{k+1}{2}, t^2\right) dt}_{I_{k2}^o}. \quad (73)$$

Then, the first integral I_{k1}^o in (73) can be computed as

$$I_{k1}^o \stackrel{(f)}{=} \int_0^{-l_{min}} e^{-\Delta y^2} y^{2m_u-1-k} \Gamma\left(\frac{k+1}{2}, y^2\right) dy \stackrel{(g)}{=} (\gamma_o - 1)! \sum_{i=0}^{\gamma_o-1} \frac{1}{i!} \int_0^{-l_{min}} e^{-(\Delta+1)y^2} y^{2m_u-1-k} dy$$

$$\stackrel{(h)}{=} \frac{(\gamma_o - 1)!}{2} \sum_{i=0}^{\gamma_o-1} \frac{(\Delta+1)^{k/2-m_u-i}}{i!} \int_0^{l_{min}^2(\Delta+1)} v^{m_u+i-k/2} e^{-v} dv$$

$$\stackrel{(i)}{=} \frac{(\gamma_o - 1)!}{2} \sum_{i=0}^{\gamma_o-1} \frac{(\Delta+1)^{k/2-m_u-i}}{i!} \gamma\left(m_u + i - \frac{k}{2}, (\Delta+1)l_{min}^2\right), \quad (74)$$

where the step (f) and step (h) are obtained by substituting $t = -y$ and $v = (\Delta+1)y^2$, respectively.

The step (g) is computed via the fact that $\Gamma(n, x) = (n-1)!e^{-x} \sum_{m=0}^{n-1} x^m/m!$ [30, Eq. (8.352.7)].

The step (i) is written via [30, Eq. (8.350.1)]. The second integral I_{k2}^o in (73) is computed as

$$I_{k2}^o = \int_0^\infty e^{-\Delta t^2} t^{2m_u-1-k} \Gamma\left(\frac{k+1}{2}, t^2\right) dt \stackrel{(j)}{=} (\gamma_o - 1)! \sum_{i=0}^{\gamma_o-1} \frac{1}{i!} \int_0^\infty t^{2m_u+2i-1-k} e^{-(\Delta+1)t^2} dt$$

$$\stackrel{(k)}{=} \frac{(\gamma_o - 1)!}{2} \sum_{i=0}^{\gamma_o-1} \frac{(\Delta+1)^{k/2-m_u-i}}{i!} \Gamma\left(m_u + i - \frac{k}{2}, (\Delta+1)l_{min}^2\right), \quad (75)$$

where the step (j) is derived via a similar technique used in the step (g), and the step (k) is evaluated by using [30, Eq. (2.33.10)]. Then, for $x - \mu_Y > 0$, I_k^o can be calculated as

$$I_k^o = \int_{l_{min}}^\infty e^{-\Delta t^2} t^{2m_u-1-k} \Gamma\left(\frac{k+1}{2}, t^2\right) dt = (\gamma_o - 1)! \sum_{i=0}^{\gamma_o-1} \frac{1}{i!} \int_{l_{min}}^\infty t^{2m_u+2i-1-k} e^{-(\Delta+1)t^2} dt$$

$$= \frac{(\gamma_o - 1)!}{2} \sum_{i=0}^{\gamma_o-1} \frac{(\Delta+1)^{k/2-m_u-i}}{i!} \Gamma\left(m_u + i - \frac{k}{2}, (\Delta+1)l_{min}^2\right). \quad (76)$$

By combining (73) and (76), I_k^o can be derived as (20). Then, for even values of k , the integral in (72) can be evaluated as

$$\begin{aligned}
I_k^e &= q \int_{l_{\min}}^{\infty} e^{-\Delta t^2} t^{2m_u-1-k} \Gamma\left(\frac{k+1}{2}, t^2\right) dt \\
&\stackrel{(l)}{=} \frac{(\gamma_e - 1)!}{2} \sum_{j=0}^{\gamma_e-1} \left[-\frac{e^{-\Delta t^2} t^{2j}}{j! \Delta^{\gamma_e-1}} \Gamma\left(\frac{k+1}{2}, t^2\right) \right]_{l_{\min}}^{\infty} - (\gamma_e - 1)! \sum_{j=0}^{\gamma_e-1} \frac{\Delta^{\gamma_e-1}}{j!} \int_{l_{\min}}^{\infty} t^{k+2j} e^{-(\Delta-1)t^2} dt \\
&= \frac{(\gamma_e - 1)!}{2} \sum_{j=0}^{\gamma_e-1} \frac{e^{-\Delta l_{\min}^2} l_{\min}^{2j}}{j! \Delta^{\gamma_e-1}} \Gamma\left(\frac{k+1}{2}, l_{\min}^2\right) - \frac{(\gamma_e - 1)!}{2} \sum_{j=0}^{\gamma_e-1} \frac{\Delta^{\gamma_e-1}}{j!} \frac{\Gamma\left(j + \frac{k}{2} + \frac{1}{2}, (\Delta+1)l_{\min}^2\right)}{(\Delta+1)^{j+k/2+1/2}},
\end{aligned} \tag{77}$$

where the step (l) is obtained by using the part-by-part integration technique.

APPENDIX D

A. The Derivation of Expectation of $\tilde{\gamma}^*$ in (27)

The expectation term in (27) can be computed as

$$\mathbb{E}[\tilde{\gamma}^*] = \mathbb{E}[\tilde{\gamma} \tilde{R}^2] = \tilde{\gamma} \mathbb{E}[(\alpha_u + \tilde{Y})^2] = \tilde{\gamma} \sum_{n=0}^2 \binom{2}{n} \mathbb{E}[\alpha_u^{(2-n)}] \mathbb{E}[\tilde{Y}^n] = \tilde{\gamma} (\sigma_u^2 + \mu_u^2 + \sigma_Y^2 + \mu_Y^2 + 2\mu_u \mu_Y), \tag{78}$$

where μ_Y , σ_Y^2 , μ_u , and σ_u^2 are given in (13a), (13b), (28a), and (28b), receptively.

B. The Derivation of Variance of $\tilde{\gamma}^*$ in (30)

The first expectation term in (30) can be evaluated as

$$\mathbb{E}[\tilde{R}^4] = \mathbb{E}[(\alpha_u + \tilde{Y})^4] = \sum_{n=0}^4 \binom{4}{n} \mathbb{E}[\alpha_u^{(4-n)}] \mathbb{E}[\tilde{Y}^n]. \tag{79}$$

Thus, the n th moment of α_u^n denoted by $\mathbb{E}[\alpha_u^n]$ can be computed as

$$\mathbb{E}[\alpha_u^n] = \int_0^{\infty} x^n f_u(x) dx = \frac{2m_u^{m_u}}{\Gamma(m_u) \xi_u^{m_u}} \int_0^{\infty} x^{2m_u+n-1} e^{-\frac{m_u x^2}{\xi_u}} dx \stackrel{(m)}{=} \frac{\xi_u^{n/2}}{\Gamma(m_u) m_u^{n/2}} \Gamma(m_u + n/2), \tag{80}$$

where the step (m) is evaluated by using [30, Eq. (2.33.10)]. Then, $\mathbb{E}[\tilde{Y}^n]$ can be derived as

$$\begin{aligned}
\mathbb{E}[\tilde{Y}^n] &= \frac{\psi}{\sqrt{2\pi\sigma_Y^2}} \int_0^{\infty} y^n e^{-\frac{(y-\mu_Y)^2}{2\sigma_Y^2}} dy \stackrel{(n)}{=} \frac{\psi}{\sqrt{\pi}} \int_{\frac{-\mu_Y}{\sqrt{2\sigma_Y^2}}}^{\infty} \left(\sqrt{2\sigma_Y^2} t + \mu_Y \right)^n e^{-t^2} dt \\
&\stackrel{(o)}{=} \frac{\psi}{2\sqrt{\pi}} \sum_{i=0}^n \binom{n}{i} \left(\sqrt{2\sigma_Y^2} \right)^{n-i} \mu_Y^i I\left(n-i, \frac{-\mu_Y}{2\sigma_Y^2}\right),
\end{aligned} \tag{81}$$

where the step (n) is due to a changing of variable and the step (o) is obtained by expanding $\left(\sqrt{2\sigma_Y^2} t + \mu_Y \right)^n$ based on n value. Moreover, $I(\cdot, \cdot)$ is given in (34).

C. The Derivation of the Asymptotic Achievable Rate (\mathcal{R}^∞) as $L \rightarrow \infty$ in (38)

When the number of IRS elements grows without bound ($L \rightarrow \infty$), μ_Y in (13a) and σ_Y^2 in (13b) can be approximated as

$$\mu_Y \approx L\bar{\mu}_Y = L \left(\sum_{n=1}^N \eta_n \sqrt{\frac{\xi_{h_n} \xi_{g_n}}{m_h m_g}} \frac{\Gamma(m_h + 1/2) \Gamma(m_g + 1/2)}{\Gamma(m_h) \Gamma(m_g)} \right), \quad (82)$$

$$\sigma_Y^2 \approx L\bar{\sigma}_Y^2 = L \left(\sum_{n=1}^N \eta_n^2 \left(\frac{\xi_{h_n} \xi_{g_n}}{m_h m_g} \right) \frac{\Gamma(m_h + 1) \Gamma(m_g + 1)}{\Gamma(m_h) \Gamma(m_g)} - \bar{\mu}_Y^2 \right), \quad (83)$$

where $\eta_n = \eta_{nl}$. Thus, the SNR term in \mathcal{R}_{ub} (36) can be asymptotically evaluated as

$$\lim_{L \rightarrow \infty} \gamma_{ub} = \lim_{L \rightarrow \infty} \bar{\gamma} L^2 \left(\frac{\sigma_u^2}{L^2} + \frac{\bar{\sigma}_Y^2}{L} + \frac{2\mu_u \bar{\mu}_Y}{L} + \frac{\mu_u^2}{L^2} + \bar{\mu}_Y^2 \right) = \bar{\gamma}_E \bar{\mu}_Y^2, \quad (84)$$

where $\bar{\gamma}_E = P_E/\sigma_w^2$ and $\lim_{L \rightarrow \infty} P = P_E/L^2$. Similarly, in the asymptotic regime, the SNR term in \mathcal{R}_{lb} (35) can be derived as

$$\lim_{L \rightarrow \infty} \gamma_{lb} = \lim_{L \rightarrow \infty} \bar{\gamma} \left(\frac{L^6 \left(\frac{\sigma_u^2}{L^2} + \frac{\bar{\sigma}_Y^2}{L} + \frac{2\mu_u \bar{\mu}_Y}{L} + \frac{\mu_u^2}{L^2} + \bar{\mu}_Y^2 \right)^3}{L^4 \left(\frac{\psi}{2\sqrt{\pi}} \bar{\mu}_Y^4 I \left(0, \frac{-\sqrt{L} \bar{\mu}_Y}{\sqrt{2\bar{\sigma}_Y^2}} \right) + \frac{\Upsilon(L^3)}{L^4} \right)} \right) = \lim_{L \rightarrow \infty} \bar{\gamma} L^2 \left(\frac{\bar{\mu}_Y^2}{\frac{\psi}{2\sqrt{\pi}} I(0, -\infty)} \right) \stackrel{(p)}{=} \bar{\gamma}_E \bar{\mu}_Y^2, \quad (85)$$

where $\Upsilon(L^3)$ is lower order ($L < 4$) terms of the expansion of the SNR in (35). Moreover, the step (p) is written by using the fact that $\lim_{L \rightarrow \infty} \psi = \lim_{L \rightarrow \infty} 1/\mathcal{Q}(-\sqrt{L} \bar{\mu}_Y/\bar{\sigma}_Y) = \lim_{L \rightarrow \infty} 1/\mathcal{Q}(-\infty) = 1$ and $I(0, -\infty) = 2\Gamma(1/2) = 2\sqrt{\pi}$. Then, the asymptotic achievable rate \mathcal{R}^∞ can be derived as given in (38).

APPENDIX E

THE DERIVATION OF THE AVERAGE SER IN (42)

The inner expectation term with respect to \tilde{Y} in (41) can be evaluated via a tight approximation [36] for the Gaussian Q -function: $\mathcal{Q}(x) \approx \exp(-cx^2 - dx)/2$, where $c=0.374$ and $d=0.777$ as

$$\mathbb{E}_{\tilde{Y}} \left[\mathcal{Q} \left(\vartheta_b(\alpha_u + \tilde{Y}) \right) \right] = \frac{1}{2} \int_0^\infty e^{-cx^2 - dx} f_{\tilde{Y}}(y) dy = \frac{\psi e^{-c\vartheta_b^2 \alpha_u^2 - d\vartheta_b \alpha_u - \frac{\mu_Y^2}{2\sigma_Y^2}}}{2\sqrt{2\pi\sigma_Y^2}} \underbrace{\int_0^\infty e^{-a_1 y^2 - a_2 y} dy}_{I_{\tilde{Y}}}, \quad (86)$$

where $a_1 = c\vartheta_b^2 + 1/2\sigma_Y^2$ and $a_2 = 2c\vartheta_b^2 \alpha_u + d\vartheta_b - \mu_Y/\sigma_Y^2$. Then, the integral $I_{\tilde{Y}}$ in (86) can be evaluated by first using a substitution $t = y + a_2/(2a_1)$ and then invoking [30, Eq. (2.33.16)]

$$\begin{aligned} I_{\tilde{Y}} &= \exp \left(\frac{a_2^2}{4a_1^2} \right) \int_0^\infty \exp \left(-a_1 \left(y + \frac{a_2}{2a_1} \right)^2 \right) dy = \exp \left(\frac{a_2^2}{4a_1^2} \right) \int_{a_2/2a_1}^\infty \exp(-a_1 t^2) dt \\ &= \frac{1}{2} \sqrt{\frac{\pi}{a_1}} \exp \left(\frac{a_2^2}{4a_1^2} \right) \operatorname{erfc} \left(\frac{a_2}{2\sqrt{a_1}} \right). \end{aligned} \quad (87)$$

Then, by substituting a_2 and (87) into (86), the inner expectation in (41) can be rewritten as

$$\mathbb{E}_{\tilde{Y}} \left[\mathcal{Q} \left(\vartheta_b(\alpha_u + \tilde{Y}) \right) \right] = \frac{\psi \exp \left(-c\vartheta_b^2 \alpha_u^2 - d\vartheta_b \alpha_u - \frac{\mu_Y^2}{2\sigma_Y^2} \right)}{4\sqrt{2\sigma_Y^2 a_1}} \exp \left(-v' \alpha_u^2 - u_1 \alpha_u \right) \operatorname{erfc} (s\alpha_u + r), \quad (88)$$

where $v' = v_1 - m_u/P_u$. Moreover, s , r , u_1 , and v_1 are defined in (44). By substituting (88) into (41), the outer expectation with respect to α_u can be written as

$$\begin{aligned} \mathbb{E}_{\alpha_u} \left[\mathbb{E}_{\tilde{Y}} \left[\mathcal{Q} \left(\vartheta_b(\alpha_u + \tilde{Y}) \right) \right] \right] &= \int_0^\infty \mathbb{E}_{\tilde{Y}} \left[\mathcal{Q} \left(\vartheta_b(\alpha_u + \tilde{Y}) \right) \right] f_u(\alpha_u) d\alpha_u \\ &= \underbrace{2\sqrt{2\pi}B \int_0^\infty \alpha_u^{2m_u-1} e^{-v_1 \left(\alpha_u + \frac{u_1}{2v_1} \right)^2} \mathcal{Q} \left(\sqrt{2}(s\alpha_u + r) \right) d\alpha_u}_{I_{\alpha_u}}, \quad (89) \end{aligned}$$

where B is defined in (44). Then, the integral I_{α_u} in (89) can be evaluated as

$$\begin{aligned} I_{\alpha_u} &= \int_0^\infty \alpha_u^{2m_u-1} e^{-v_1 \left(\alpha_u + \frac{u_1}{2v_1} \right)^2} \mathcal{Q} \left(\sqrt{2}(s\alpha_u + r) \right) d\alpha_u \quad (90) \\ &\stackrel{(q)}{=} \frac{-1}{2} \sum_{k=0}^{2m_u-1} \left(\frac{-u_1}{2v_1} \right)^{2m_u-1-k} \Gamma(\gamma_b) \left[\mathcal{Q} \left(\sqrt{2}(s\alpha_u + r) \right) e^{-v_1 \left(\alpha_u + \frac{u_1}{2v_1} \right)^2} \sum_{i=0}^{\gamma_b-1} \frac{(\alpha_u + u_1/2v_1)^{2i}}{i!v_1^{\gamma_b-i}} \right]_0^\infty \\ &\quad - \frac{s}{2\sqrt{\pi}} \sum_{k=0}^{2m_u-1} \left(\frac{-u_1}{2v_1} \right)^{2m_u-1-k} \Gamma(\gamma_b) \sum_{i=0}^{\gamma_b-1} \frac{1}{i!v_1^{\gamma_b-i}} \int_0^\infty \left(\alpha_u + \frac{u_1}{2v_1} \right)^{2i} e^{-v_1 \left(\alpha_u + \frac{u_1}{2v_1} \right)^2 - (s\alpha_u + r)^2} d\alpha_u \\ &= \frac{\mathcal{Q}(\sqrt{2}r)}{2} \sum_{k=0}^{2m_u-1} \left(\frac{-u_1}{2v_1} \right)^{2m_u-1-k} \Gamma(\gamma_b) \sum_{i=0}^{\gamma_b-1} \frac{(u_1/2v_1)^{2i}}{i!v_1^{\gamma_b-i}} \\ &\quad - \frac{s}{2\sqrt{\pi}} \sum_{k=0}^{2m_u-1} \left(\frac{-u_1}{2v_1} \right)^{2m_u-1-k} \Gamma(\gamma_b) \sum_{i=0}^{\gamma_b-1} \frac{1}{i!v_1^{\gamma_b-i}} \underbrace{\int_0^\infty \left(\alpha_u + \frac{u_1}{2v_1} \right)^{2i} e^{-v_1 \left(\alpha_u + \frac{u_1}{2v_1} \right)^2 - (s\alpha_u + r)^2} d\alpha_u}_{I_{\alpha'_u}}, \end{aligned}$$

where $\gamma_b = (k+1)/2$. The step (q) is written by using the part-by-part integration technique.

Then, the integral $I_{\alpha'_u}$ can be rearranged as follows:

$$\begin{aligned} I_{\alpha'_u} &= e^{\frac{u_2^2}{4v_2} - \frac{u_1^2}{4v_1} - r} \int_0^\infty \left(\alpha_u + \frac{u_1}{2v_1} \right)^{2i} e^{-v_2 \left(\alpha_u + \frac{u_2}{2v_2} \right)^2} d\alpha_u \\ &\stackrel{(r)}{=} e^{\frac{u_2^2}{4v_2} - \frac{u_1^2}{4v_1} - r} \sum_{j=0}^{2i} q_b^{2i-j} \int_{\frac{u_2}{2v_2}}^\infty t^j e^{-v_2 t^2} dt = e^{\frac{u_2^2}{4v_2} - \frac{u_1^2}{4v_1} - r} \sum_{j=0}^{2i} q_b^{2i-j} I_b, \quad (91) \end{aligned}$$

where $q_b = u_1/2v_1 - u_2/2v_2$ and I_b is defined in (43). Further, the step (r) is obtained via the substitution $t = \alpha_u + u_2/(2v_2)$. Finally, u_2 and v_2 are defined in (44).

APPENDIX F

THE DERIVATION OF P_{out}^∞ IN (47) AND \bar{P}_e^∞ IN (53)

From (67) in Appendix A, the PDF of $z_{nl} = \alpha_{h_{nl}} \alpha_{g_{nl}}$ can be written as

$$f_{z_{nl}}(x) = \alpha' x^{m_s+m_l-1} \mathcal{K}_{m_s-m_l} \left(2x \sqrt{m_s m_l / (\xi_{s_n} \xi_{l_n})} \right), \quad (92)$$

where α' is given in (50b), $m_s = \min(m_h, m_g)$, and $m_l = \max(m_h, m_g)$. Moreover, ξ_{s_n} and ξ_{l_n} are the scaling parameters of the respective channel models (3). The moment generating function (MGF) of z_{nl} can be derived by evaluating the Laplace transform of $f_{z_{nl}}(x)$ as [29]

$$\begin{aligned} \mathcal{M}_{z_{nl}}(s) &= \int_0^\infty f_{z_{nl}}(x) \exp(-sx) dx = \alpha' \int_0^\infty x^{m_s+m_l-1} e^{-sx} \mathcal{K}_{m_s-m_l} \left(2x \sqrt{m_s m_l / (\xi_{s_n} \xi_{l_n})} \right) dx \quad (93) \\ &\stackrel{(s)}{=} \frac{\alpha' \sqrt{\pi} (2b_n)^{(m_s-m_l)} \Gamma(2m_s) \Gamma(2m_l)}{\Gamma(m_s + m_l + 1/2)} (s+b_n)^{2m_s} F \left(2m_s, m_s-m_l+\frac{1}{2}; m_s+m_l+\frac{1}{2}; \frac{s-b_n}{s+b_n} \right), \end{aligned}$$

where $b_n = 2\sqrt{m_s m_l / (\xi_{s_n} \xi_{l_n})}$. In (93), the step (s) is derived by using [30, Eq. (6.621.3)]. The behavior of the PDF of z_{nl} at the origin is governed by the asymptotic value of $\mathcal{M}_{z_{nl}}(s)$ as $s \rightarrow \infty$ [37]. To this end, by using the fact that $\lim_{s \rightarrow \infty} (s-b_n)/(s+b_n) \rightarrow 1$, and we invoke [42, Eq. (15.4.21)] for $m_s = m_l$ and [30, Eq. (9.122.1)] for $m_s < m_l$ to evaluate $\mathcal{M}_{z_{nl}}(s)$ when $s \rightarrow \infty$ as follows:

$$\mathcal{M}_{z_{nl}}^\infty(s) = \theta_n s^{-2m_s}, \quad (94)$$

where θ_n is defined in (50a). Thus, the MGF of $Y = \sum_{n=1}^N \sum_{l=1}^L \eta_{nl} z_{nl}$ as $s \rightarrow \infty$ is given by

$$\mathcal{M}_Y^\infty(s) = \prod_{n=1}^N \prod_{l=1}^L \eta_{nl} \theta_n s^{-2m_s} = \Phi(N, L) s^{-2m_s N L}, \quad (95)$$

where $\Phi(N, L)$ is given in (49). The PDF of the direct channel envelope (u) is expanded at the origin via the Maclaurin series expansion of the exponential function [30, Eq. (0.318.2)] as

$$\begin{aligned} f_{\alpha_u}(x) &= \frac{2m_u^{m_u} x^{2m_u-1}}{\Gamma(m_u) \xi_u^{m_u}} \exp\left(\frac{-x^2}{\xi_u}\right) = \frac{2m_u^{m_u} x^{2m_u-1}}{\Gamma(m_u) \xi_u^{m_u}} \sum_{k=0}^{\infty} \frac{1}{k!} \left(\frac{-x^2}{\xi_u}\right)^k \\ &= \frac{2m_u^{m_u} x^{2m_u-1}}{\Gamma(m_u) \xi_u^{m_u}} \left(1 - \frac{x^2}{\xi_u} + \frac{x^4}{2\xi_u^2} - \frac{x^6}{6\xi_u^3} + \dots\right). \end{aligned} \quad (96)$$

Then, the PDF of the direct channel envelope (u) for $x \rightarrow 0^+$ can be approximated as

$$f_{\alpha_u}^{0+}(x) = \frac{2m_u^{m_u} x^{2m_u-1}}{\Gamma(m_u) \xi_u^{m_u}} + \mathcal{O}(x^{2m_u}). \quad (97)$$

Via the Laplace transform of (97), we obtain the asymptotic MGF of α_u as [30, Eq. (17.13.2)]

$$\mathcal{M}_{\alpha_u}^\infty(s) = \frac{2m_u^{m_u} \Gamma(2m_u)}{\Gamma(m_u) \xi_u^{m_u}} s^{-2m_u}. \quad (98)$$

Then, the asymptotic MGF of $R = \alpha_u + Y$ for $s \rightarrow \infty$ can be derived as

$$\mathcal{M}_R^\infty(s) = \mathcal{M}_Y^\infty(s) \mathcal{M}_{\alpha_u}^\infty(s) = \frac{\Phi(N, L) 2m_u^{m_u} \Gamma(2m_u)}{\Gamma(m_u) \xi_u^{m_u}} s^{-2m_s N L - 2m_u}, \quad (99)$$

where $\Phi(N, L)$ is defined in (49). By taking inverse Laplace transform of (99) [30], the PDF of R for $x \rightarrow 0^+$ can be computed as

$$f_R^{0+}(x) \stackrel{(t)}{=} \frac{\Phi(N, L) 2m_u^{m_u} \Gamma(2m_u)}{\Gamma(m_u) \xi_u^{m_u} \Gamma(2m_s NL + 2m_u)} x^{2m_s NL + 2m_u - 1} + \mathcal{O}(x^{2m_s NL + 2m_u}), \quad (100)$$

where the step (t) is written via [30, Eq. (17.13.3)]. Next, the CDF of R for $x \rightarrow 0^+$ is given as

$$\begin{aligned} F_R^{0+}(x) &= \int_0^x f_R^{0+}(u) du = \int_0^x \frac{\Phi(N, L) 2m_u^{m_u} \Gamma(2m_u)}{\Gamma(m_u) \xi_u^{m_u} \Gamma(2m_s NL + 2m_u)} u^{2m_s NL + 2m_u - 1} du + \mathcal{O}(u^{2m_s NL + 2m_u}) \\ &= \frac{\Phi(N, L) m_u^{m_u} \Gamma(2m_u)}{G_d \Gamma(m_u) \xi_u^{m_u} \Gamma(2G_d)} x^{2G_d} + \mathcal{O}(x^{2G_d+1}), \end{aligned} \quad (101)$$

where $G_d = m_s NL + m_u$. Then, the CDF of $\gamma^* = \bar{\gamma} R^2$ for $x \rightarrow 0^+$ is approximated as [29]

$$F_{\gamma^*}^{0+}(x) = \Pr(\gamma^* \leq x) \approx F_R^{0+}(\sqrt{x/\bar{\gamma}}) = \frac{\Phi(N, L) m_u^{m_u} \Gamma(2m_u)}{G_d \Gamma(m_u) \xi_u^{m_u} \Gamma(2G_d)} \left(\frac{x}{\bar{\gamma}}\right)^{G_d} + \mathcal{O}\left(\left(\frac{x}{\bar{\gamma}}\right)^{G_d+1}\right). \quad (102)$$

Thereby, the asymptotic outage probability can be computed as

$$P_{out}^\infty \approx F_{\gamma^*}^{0+}(\gamma_{th}) = \Omega \Phi(N, L) \left(\frac{\gamma_{th}}{\bar{\gamma}}\right)^{G_d} + \mathcal{O}\left(\left(\frac{\gamma_{th}}{\bar{\gamma}}\right)^{G_d+1}\right), \quad (103)$$

where Ω is given in (49). Finally, the asymptotic average BER can be derived as follows:

$$\begin{aligned} P_e^\infty &= \int_0^\infty \omega \mathcal{Q}(\sqrt{\vartheta x}) f_{\gamma^*}^{0+}(x) dx = \frac{\omega}{2} \sqrt{\frac{\vartheta}{2\pi}} \int_0^\infty x^{-1/2} \exp\left(\frac{-\vartheta x}{2}\right) F_{\gamma^*}^{0+}(x) dx \\ &= \frac{\omega}{2} \sqrt{\frac{\vartheta}{2\pi}} \frac{\Phi(N, L) m_u^{m_u} \Gamma(2m_u)}{G_d \Gamma(m_u) \xi_u^{m_u} \Gamma(2G_d)} \bar{\gamma}^{-G_d} \int_0^\infty x^{G_d-1/2} \exp\left(\frac{-\vartheta x}{2}\right) dx + \mathcal{O}\left(\left(\frac{x}{\bar{\gamma}}\right)^{G_d+1}\right) \\ &\stackrel{(u)}{=} \Lambda \Phi(N, L) \bar{\gamma}^{-G_d} + \mathcal{O}(\bar{\gamma}^{-(G_d+1)}), \end{aligned} \quad (104)$$

where Λ is given in (54) and the step (u) is computed via [30, Eq. (3.326.2)].

REFERENCES

- [1] D. L. Galappaththige, D. Kudathanthirige, and G. Amarasureiya, "Performance Analysis of Distributed Intelligent Reflective Surface Aided Communications," in *IEEE Global Commun. Conf. (GLOBECOM)*, 2020, pp. 1–6.
- [2] C. Liaskos *et al.*, "A New Wireless Communication Paradigm Through Software-Controlled Metasurfaces," *IEEE Commun. Mag.*, vol. 56, no. 9, pp. 162–169, 2018.
- [3] M. D. Renzo *et al.*, "Smart Radio Environments Empowered by Reconfigurable AI Meta-Surfaces: An Idea Whose Time Has Come," *EURASIP J. Wireless Commun. Net.*, May 2019.
- [4] T. Sekitani *et al.*, "Stretchable Active-Matrix Organic Light-Emitting Diode Display Using Printable Elastic Conductors," *Nature Materials*, vol. 11, no. 11, pp. 494–499, 2009.
- [5] S. Zhang, Q. Wu, S. Xu, and G. Y. Li, "Fundamental Green Tradeoffs: Progresses, Challenges, and Impacts on 5G Networks," *IEEE Commun. Surveys Tuts.*, vol. 19, no. 1, pp. 33–56, 2017.
- [6] E. Basar *et al.*, "Wireless Communications Through Reconfigurable Intelligent Surfaces," *IEEE Access*, vol. 7, pp. 116 753–116 773, 2019.
- [7] W. Tang *et al.*, "Wireless Communications with Reconfigurable Intelligent Surface: Path Loss Modeling and Experimental Measurement," *IEEE Trans. Wireless Commun.*, vol. 20, no. 1, pp. 421–439, 2021.

- [8] J. Chen, Y. Liang, Y. Pei, and H. Guo, "Intelligent Reflecting Surface: A Programmable Wireless Environment for Physical Layer Security," *IEEE Access*, vol. 7, pp. 82 599–82 612, 2019.
- [9] D. Kudathanthirige, D. Gunasinghe, and G. Amarasinghe, "Performance Analysis of Intelligent Reflective Surfaces for Wireless Communication," in *IEEE Int. Conf. Commun. (ICC)*, June 2020, pp. 1–6.
- [10] E. Basar, "Transmission Through Large Intelligent Surfaces: A New Frontier in Wireless Communications," *European Conf. Netw. and Commun. (EuCNC)*, pp. 112–117, 2019.
- [11] Y. Han, W. Tang, S. Jin, C. Wen, and X. Ma, "Large Intelligent Surface-Assisted Wireless Communication Exploiting Statistical CSI," *IEEE Trans. Veh. Technol.*, vol. 68, no. 8, pp. 8238–8242, Aug 2019.
- [12] M. Jung, W. Saad, Y. Jang, G. Kong, and S. Choi, "Reliability Analysis of Large Intelligent Surfaces (LISs): Rate Distribution and Outage Probability," *IEEE Wireless Commun. Lett.*, vol. 8, no. 6, pp. 1662–1666, 2019.
- [13] M. Jung, W. Saad, M. Debbah, and C. S. Hong, "On the Optimality of Reconfigurable Intelligent Surfaces (RISs): Passive Beamforming, Modulation, and Resource Allocation," *IEEE Trans. Wireless Commun.*, vol. 20, no. 7, pp. 4347–4363, 2021.
- [14] S. Hu and F. Rusek, "Spherical Large Intelligent Surfaces," *IEEE Int. Conf. Acoust., Speech and Signal Process.*, pp. 8673–8677, 2020.
- [15] C. Psomas, I. Chrysovergis, and I. Krikidis, "Random Rotation-Based Low-Complexity Schemes for Intelligent Reflecting Surfaces," in *2020 IEEE 31st Ann. Int. Symp. Personal, Indoor and Mobile Radio Commun.*, 2020, pp. 1–6.
- [16] Q. Wu and R. Zhang, "Intelligent Reflecting Surface Enhanced Wireless Network via Joint Active and Passive Beamforming," *IEEE Trans. Wireless Commun.*, vol. 18, no. 11, pp. 5394–5409, 2019.
- [17] —, "Beamforming Optimization for Wireless Network Aided by Intelligent Reflecting Surface with Discrete Phase Shifts," *IEEE Trans. Commun.*, vol. 68, no. 3, pp. 1838–1851, 2020.
- [18] C. Huang, A. Zappone, G. C. Alexandropoulos, M. Debbah, and C. Yuen, "Reconfigurable Intelligent Surfaces for Energy Efficiency in Wireless Communication," *IEEE Trans. Wireless Commun.*, vol. 18, no. 8, pp. 4157–4170, 2019.
- [19] S. Abeywickrama, R. Zhang, and C. Yuen, "Intelligent Reflecting Surface: Practical Phase Shift Model and Beamforming Optimization," in *IEEE Int. Conf. Commun. (ICC)*, 2020, pp. 1–6.
- [20] S. Zhang and R. Zhang, "Intelligent Reflecting Surface Aided Multiple Access: Capacity Region and Deployment Strategy," in *2020 IEEE 21st Int. Workshop Signal Process. Adv. in Wireless Commun. (SPAWC)*, 2020, pp. 1–5.
- [21] C. Guo, Y. Cui, F. Yang, and L. Ding, "Outage Probability Analysis and Minimization in Intelligent Reflecting Surface-Assisted MISO Systems," *IEEE Commun. Lett.*, vol. 24, no. 7, pp. 1563–1567, 2020.
- [22] M. Cui, G. Zhang, and R. Zhang, "Secure Wireless Communication via Intelligent Reflecting Surface," *IEEE Wireless Commun. Lett.*, vol. 8, no. 5, pp. 1410–1414, 2019.
- [23] X. Guan, Q. Wu, and R. Zhang, "Intelligent Reflecting Surface Assisted Secrecy Communication: Is Artificial Noise Helpful or Not?" *IEEE Wireless Commun. Lett.*, vol. 9, no. 6, pp. 778–782, 2020.
- [24] Y. Gao, J. Xu, W. Xu, D. W. K. Ng, and M. S. Alouini, "Distributed IRS With Statistical Passive Beamforming for MISO Communications," *IEEE Commun. Lett.*, vol. 10, no. 2, pp. 221–225, 2021.
- [25] W. Mei and R. Zhang, "Cooperative Multi-Beam Routing for Multi-IRS Aided Massive MIMO," in *IEEE Int. Conf. Commun. (ICC)*, 2021, pp. 1–6.
- [26] —, "Multi-Beam Multi-Hop Routing for Intelligent Reflecting Surfaces Aided Massive MIMO," *IEEE Trans. Wireless Commun.*, pp. 1–1, 2021.

- [27] L. Yang, F. Meng, Q. Wu, D. B. da Costa, and M.-S. Alouini, "Accurate Closed-Form Approximations to Channel Distributions of RIS-Aided Wireless Systems," *IEEE Commun. Lett.*, vol. 9, no. 11, pp. 1985–1989, 2020.
- [28] L. Yang, Y. Yang, D. B. d. Costa, and I. Trigui, "Outage Probability and Capacity Scaling Law of Multiple RIS-Aided Networks," *IEEE Commun. Lett.*, vol. 10, no. 2, pp. 256–260, 2021.
- [29] A. Papoulis and S. U. Pillai, *Probability, Random Variables, and Stochastic Processes*, 4th ed. McGraw Hill, 2002.
- [30] I. Gradshteyn and I. Ryzhik, *Table of Integrals, Series, and Products*, 7th ed. Academic Press, 2007.
- [31] E. Björnson and L. Sanguinetti, "Rayleigh Fading Modeling and Channel Hardening for Reconfigurable Intelligent Surfaces," *IEEE Wireless Commun. Lett.*, vol. 10, no. 4, pp. 830–834, 2021.
- [32] Q. Wu and R. Zhang, "Towards Smart and Reconfigurable Environment: Intelligent Reflecting Surface Aided Wireless Network," *IEEE Commun. Mag.*, vol. 58, no. 1, pp. 106–112, 2020.
- [33] Q. Zhang, S. Jin, K.-K. Wong, H. Zhu, and M. Matthaiou, "Power Scaling of Uplink Massive MIMO Systems with Arbitrary-Rank Channel Means," *IEEE J. Sel. Areas Signal Process.*, vol. 8, no. 5, pp. 966–981, Oct. 2014.
- [34] E. Björnson, z. Özdogan, and E. G. Larsson, "Reconfigurable Intelligent Surfaces: Three Myths and Two Critical Questions," *IEEE Commun. Mag.*, vol. 58, no. 12, pp. 90–96, 2020.
- [35] J. Proakis, *Digital Communications*, 4th ed. New York:McGraw-Hill, Inc., 2001.
- [36] A. Mastin and P. Jaillet, "Log-Quadratic Bounds for the Gaussian Q-function," *arXiv e-prints*, 2013.
- [37] Z. Wang and G. B. Giannakis, "A Simple and General Parameterization Quantifying Performance in Fading Channels," *IEEE Trans. Commun.*, vol. 51, no. 8, pp. 1389–1398, Aug. 2003.
- [38] S. Haykin and M. Moher, *Communication Systems*, 5th ed. Wiley India Pvt. Limited, 2009.
- [39] M.-A. Badiu and J. P. Coon, "Communication Through a Large Reflecting Surface With Phase Errors," *IEEE Wireless Commun. Lett.*, vol. 9, no. 2, pp. 184–188, 2020.
- [40] M. Di Renzo *et al.*, "Smart Radio Environments Empowered by Reconfigurable Intelligent Surfaces: How It Works, State of Research, and The Road Ahead," *IEEE J. Sel. Areas Commun.*, vol. 38, no. 11, pp. 2450–2525, 2020.
- [41] T. L. Marzetta, E. G. Larsson, H. Yang, and H. Q. Ngo, *Fundamentals of Massive MIMO*. Cambridge University Press, Cambridge, UK, 2016.
- [42] D. W. Lozier, "NIST Digital Library of Mathematical Functions," *Annals of Mathematics and Artificial Intelligence*, vol. 38, no. 1-3, pp. 105–119, May 2003. [Online]. Available: <https://doi.org/10.1023/A:1022915830921>